

Recoil- $\beta$  tagging study of the  $N = Z$  nucleus  $^{66}\text{As}$ 

P. Ruotsalainen,<sup>1,\*</sup> C. Scholey,<sup>1</sup> R. Julin,<sup>1</sup> K. Hauschild,<sup>1,2</sup> K. Kaneko,<sup>3</sup> B. S. Nara Singh,<sup>4</sup> R. Wadsworth,<sup>4</sup> D. G. Jenkins,<sup>4</sup> T. S. Brock,<sup>4</sup> P. T. Greenlees,<sup>1</sup> J. Henderson,<sup>4</sup> U. Jakobsson,<sup>1</sup> P. Jones,<sup>1,†</sup> S. Juutinen,<sup>1</sup> S. Ketelhut,<sup>1,‡</sup> M. Leino,<sup>1</sup> N. M. Lumley,<sup>5</sup> P. J. R. Mason,<sup>6</sup> P. Nieminen,<sup>1</sup> M. Nyman,<sup>1</sup> I. Paterson,<sup>4</sup> P. Peura,<sup>1</sup> M. G. Procter,<sup>5</sup> P. Rauhila,<sup>1</sup> J. Sarén,<sup>1</sup> J. Sorri,<sup>1</sup> and J. Uusitalo<sup>1</sup>

<sup>1</sup>*Department of Physics, University of Jyväskylä, P.O. Box 35, FI-40014 Jyväskylä, Finland*

<sup>2</sup>*CSNSM, IN2P3-CNRS, F-91405 Orsay Campus, France*

<sup>3</sup>*Department of Physics, Kyushu Sangyo University, Fukuoka 813-8503, Japan*

<sup>4</sup>*Department of Physics, University of York, Heslington, York YO10 5DD, United Kingdom*

<sup>5</sup>*Schuster Laboratory, University of Manchester, Manchester M13 9PL, United Kingdom*

<sup>6</sup>*Department of Physics, Faculty of Engineering and Physical Sciences, University of Surrey, Guildford GU2 7XH, United Kingdom*

(Received 29 April 2013; revised manuscript received 27 June 2013; published 21 August 2013)

An in-beam study has been performed to further investigate the known isomeric decays and to identify  $T = 1$  excited states in the medium-heavy  $N = Z = 33$  nucleus  $^{66}\text{As}$ . The fusion-evaporation reaction  $^{40}\text{Ca}(^{28}\text{Si}, pn)^{66}\text{As}$  was employed at beam energies of 75 and 83 MeV. The half-lives and ordering of two known isomeric states in  $^{66}\text{As}$  have been determined with improved accuracy. In addition, several prompt  $\gamma$ -ray transitions from excited states, both bypassing and decaying to the isomeric states in  $^{66}\text{As}$ , have been observed. Most importantly, candidates for the  $4^+ \rightarrow 2^+$  and  $6^+ \rightarrow 4^+$  transitions in the  $T = 1$  band have been identified. The results are compared with shell-model calculations using the modern JUN45 interaction in the  $pf_{5/2}g_{9/2}$  model space.

DOI: [10.1103/PhysRevC.88.024320](https://doi.org/10.1103/PhysRevC.88.024320)

PACS number(s): 23.20.Lv, 21.60.Cs, 23.40.-s, 27.50.+e

## I. INTRODUCTION

Self-conjugate odd-odd  $N = Z$  nuclei are interesting for various reasons, one of which is the competition between isospin  $T = 0$  and  $T = 1$  states, fundamentally arising from neutron-neutron ( $nn$ ) or proton-proton ( $pp$ ) ( $T = 1$ ) and neutron-proton ( $np$ ) ( $T = 1$  or  $T = 0$ ) correlations. In  $N = Z$  nuclei, neutrons and protons occupy the same single-particle orbits, which leads to the maximal overlap of their wave functions. This may lead to enhanced  $np$  pairing correlations in the isoscalar  $T = 0$  channel. However, for medium-mass  $N = Z$  nuclei there is no clear evidence of the strong  $T = 0$ ,  $np$  correlations until the  $A \sim 90$  mass region is reached [1–3].

Owing to the charge symmetry and charge independence of the strong nuclear force, any state that can be constructed in the even-even  $pp$  and  $nn$  systems ( $Z = N + 2$  or  $Z = N - 2$ ) has to exist also in the odd-odd ( $N = Z$ )  $np$  system. This fact leads to the concept of isospin symmetry, which implies that a set of states with the same isospin quantum number ( $T = 1$ ) within an isobaric multiplet, are degenerate. However, the observed differences in the excitation energies of the isobaric analog states (IAS) originate from isospin nonconserving forces, such as the Coulomb interaction [4]. The energy differences, called Coulomb energy differences (CED), between the IAS can be used to probe the microscopic and macroscopic structure of nuclei. CED have been used to provide information on the

alignment of the valence nucleons [5], shape changes as a function of spin [6], and the evolution of nuclear radii along the yrast line [7].

Two isomeric states have been previously identified in  $^{66}\text{As}$  [8]. In more recent studies, the decay of the isomers was used as a tag to identify excited states above the isomeric states [9] and new prompt  $\gamma$  rays were associated with  $^{66}\text{As}$ , without the ability to observe delayed transitions, in Ref. [10]. In the current work, both the isomeric and the prompt  $T = 0$  and  $T = 1$  structures have been studied. The half-lives and ordering of the isomeric states have been determined with improved accuracy and internal conversion coefficients have been deduced for the transitions deexciting the isomers, allowing the determination of the corresponding experimental  $B(E2)$  transition strengths. Recent experimental [10] and theoretical [11] work has investigated the CED in the  $A = 66$  ( $^{66}\text{As}/^{66}\text{Ge}$ ) and  $A = 70$  ( $^{70}\text{Br}/^{70}\text{Se}$ ) systems. The present work agrees with some of the findings reported in Ref. [10], but differs for the  $T = 1$ ,  $I^\pi = 6^+$  state resulting in a positive CED behavior.

The odd-odd  $N = Z$  nuclei in the mass  $A \sim 60$ –70 region provide an opportunity to test shell-model (SM) interactions and model spaces for these midmass nuclei. In the present work SM calculations have been performed using the modern JUN45 interaction [12] and a  $pf_{5/2}g_{9/2}$  model space. The experimental results are compared with the SM predictions in terms of level energies, CED, and  $B(E2)$  values.

\*panu.ruotsalainen@jyu.fi

<sup>†</sup>Present address: iThemba Laboratory for Accelerator Based Sciences, P.O. Box 722, 7129 Somerset West, South Africa.

<sup>‡</sup>Present address: TRIUMF, Westbrook Mall, Vancouver, BC, Canada V6T 2A3.

## II. EXPERIMENTAL DETAILS

Experimental studies of  $N = Z$  nuclei in the  $fpg$  shell region are very challenging as they lie rather close to the

proton-drip line where the production cross sections in fusion-evaporation reactions become very small compared to the lighter  $fp$  shell nuclei. In addition, in the case of odd-odd  $N = Z$  nuclei, the  $T = 1$  bands become rapidly nonyrast, which leads to the fact that they are weakly populated. All this means that new experimental approaches need to be investigated. The recent development of the recoil- $\beta$ -tagging (RBT) technique [6,13,14] provides a tool to extend the use of tagging methodology to the region of exotic medium-mass nuclei around the  $N = Z$  line. In the RBT method, the recoil formed via fusion-evaporation reaction is identified by correlating a  $\beta$  particle originating from the  $\beta$  decay to the recoil from which it originated. This is not straightforward because the  $\beta$ -decay properties are not generally suitable for tagging purposes, owing to the long half-lives and continuous energy distributions of  $\beta$  particles. However, the medium-heavy odd-odd  $N = Z$  and  $N < Z$  nuclei have  $\beta$ -decay properties that are suitable for RBT and can thereby serve as a clean tag for prompt or delayed  $\gamma$ -ray transitions. Specifically, the odd-odd  $N = Z$  nuclei, like  $^{66}\text{As}$  studied here, are Fermi superallowed  $\beta$  emitters, which have relatively short half-lives ( $\sim 100$  ms) and high values of  $\beta$ -particle energy distributions up to  $\sim 10$  MeV. This differs from the other nuclei in the region, which have half-lives from seconds to hours and  $\beta$ -end-point energies reaching values only up to  $\sim 3$  MeV.

The experiment was performed at the Accelerator Laboratory of the University of Jyväskylä, where the beam was delivered by the K-130 cyclotron. The  $^{40}\text{Ca}(^{28}\text{Si},pn)^{66}\text{As}$  reaction was employed at beam energies of 83 MeV (40 h of irradiation time) and 75 MeV (120 h of irradiation time) to populate excited states in  $^{66}\text{As}$ . The  $^{28}\text{Si}$  beam impinged on a  $^{nat}\text{Ca}$  target rolled to a thickness of  $800 \mu\text{g}/\text{cm}^2$ , with an average beam intensity of 5 pA. Prompt  $\gamma$  rays were detected at the target position by the JUROGAM II  $\gamma$ -ray spectrometer consisting of 24 EUROGAM Clover [15] and 15 EUROGAM Phase 1 [16] or GASP [17] type of Compton-suppressed germanium detectors with a total photopeak efficiency of 6.1% at 1.33 MeV. Fusion-evaporation recoils were separated from the primary beam and other unwanted reaction products by the gas-filled recoil separator RITU [18,19].

After separation, reaction products enter the GREAT spectrometer [20] located at the focal plane of RITU. In GREAT, reaction products first pass through a multiwire proportional counter (MWPC) and implant into a pair of  $700\text{-}\mu\text{m}$ -thick double-sided silicon strip detectors (DSSDs), where the subsequent  $\beta$  decays of the recoils are also detected. Each of the DSSDs comprises an active area of  $60 \times 40$  mm with a strip pitch of 1 mm, providing 4800 pixels in total. The fusion recoils are distinguished from scattered beam and other unwanted reaction products by energy-loss information obtained from the MWPC and time-of-flight information obtained between the DSSD and MWPC. In addition, the GREAT spectrometer has clover- and planar-type germanium detectors installed around the DSSDs to observe delayed  $\gamma$ -ray radiation. The clover detector is situated above the GREAT chamber, whereas the planar is placed directly behind the DSSDs in the vacuum chamber. The planar germanium detector was also used for detecting the high-energy  $\beta$  particles in coincidence with the energy-loss signal obtained from the

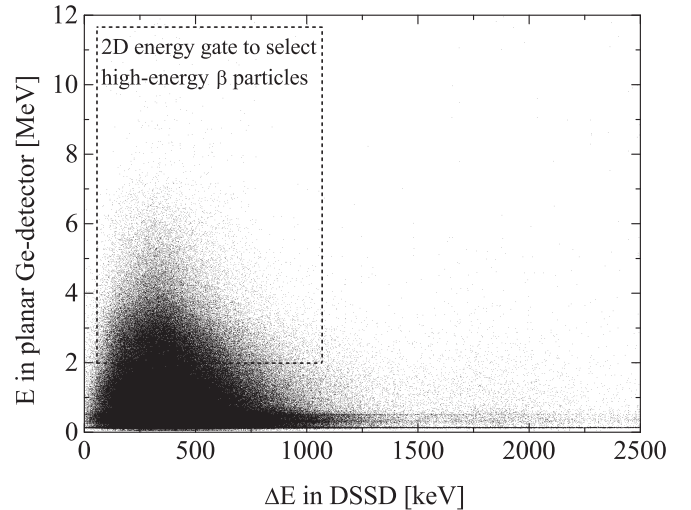


FIG. 1. Identification matrix for high-energy  $\beta$  particles. The energy-loss information ( $\Delta E$ ) is obtained from the DSSD ( $x$  axis) and full energy information ( $E$ ) from the planar Ge detector ( $y$  axis). A two-dimensional energy gate can be applied to select  $\beta$  particles to be correlated with recoils within a correlation time of 300 ms. The low-energy detection threshold can be varied to achieve better statistics or cleanliness of the tagged spectra.

DSSD. The signals from each detector channel received a time stamp with a 10-ns precision from the triggerless total data readout (TDR) [21] data acquisition system and could be sorted on or off line according to the desired time and energy conditions. The software packages GRAIN [22] and RADWARE [23,24] were used to analyze the collected data.

### A. The recoil- $\beta$ tagging method

The exceptional  $\beta$ -decay properties of  $^{66}\text{As}$  are suitable for successful tagging owing to the short half-life of  $\sim 96$  ms [25–27] and high  $\beta^+$ -end-point energy of  $\sim 9.6$  MeV [28,29]. This results from the fact that the ground state of  $^{66}\text{As}$  has a Fermi superallowed  $\beta$  decay to the daughter  $^{66}\text{Ge}$ . The identification of high-energy  $\beta^+$  particles is carried out by detecting coincidences between the DSSD and the planar germanium detector within a 0- to 200-ns time gate. These detectors can provide  $\Delta E$  and full  $E$  information for these particles, respectively. From the  $\Delta E$ – $E$  matrix, illustrated in Fig. 1, the events to be correlated with a recoil, which occurred in the same pixel of the DSSD as the  $\beta$  decay, within a maximum correlation time of 300 ms, are selected by setting a two-dimensional energy gate. The size of the gate can be varied to optimize for maximum statistics or for the cleanliness of the tagged spectra. The low-energy threshold for the  $\beta^+$  particles was varied between 0.5–5 MeV during the analysis of the correlated  $\gamma$ -ray transitions. The transitions originating from excited states in  $^{66}\text{As}$  were first identified with very strict tagging conditions, i.e., with high  $\beta^+$ -particle energy threshold of the order of  $\sim 3$ –5 MeV. The threshold was then relaxed to  $\sim 0.5$ –3 MeV in order to perform prompt  $\gamma$  and angular distribution analysis with sufficient statistics.

### B. Angular distributions of $\gamma$ -ray transitions

The multiplicities of the strongest  $\gamma$ -ray transitions originating from  $^{66}\text{As}$  were deduced by means of angular distributions and angular distribution ratios. JUROGAM II germanium detectors are divided into four rings at angles of  $75.5^\circ$  (12 detectors),  $104.5^\circ$  (12 detectors),  $133.6^\circ$  (10 detectors), and  $157.6^\circ$  (5 detectors) with respect to the beam direction. For  $\gamma$ -ray angular distributions,  $\beta$ -tagged,  $\beta$ - and isomer-tagged, or only isomer-tagged prompt events were sorted separately into four spectra corresponding to different rings of detectors. The intensities of the  $\gamma$  rays of interest were extracted from each spectrum and normalized by the detection efficiency of the corresponding ring. The reduced angular distribution function  $W(\theta) = A_0[1 + A_2 P_2(\cos\theta)]$ , where  $A_0$  and  $A_2$  are the angular distribution coefficients used as free fitting parameters and  $P_2(\cos\theta)$  is the second-order Legendre polynomial, was fitted to the detection angle vs  $\gamma$ -ray intensity plot. The fitted parameter  $A_2$  was used to deduce the transition multipolarity: a positive value indicating a quadrupole character and a negative value a dipole character.

The angular distribution ratios ( $R$ ) were deduced by two methods depending on the  $\gamma$ -ray transition intensity and cleanliness. The  $R$  values were extracted from three  $\gamma\gamma$  matrices, which were formed by sorting  $\beta$ -tagged coincidence events with  $(133.6^\circ + 157.6^\circ)$  vs (all angles),  $(104.5^\circ)$  vs (all angles), and  $(75.5^\circ)$  vs (all angles) combinations. By setting the same energy gates on the  $y$  axis (all angles) in each matrix, three coincidence spectra were formed representing the aforementioned detection angles. The intensity of the  $\gamma$  ray to be studied was again extracted from the spectra and normalized for the detection efficiency. The angular distribution ratio was calculated with the formulas  $R_1 = I_\gamma(133.6^\circ + 157.6^\circ)/I_\gamma(104.5^\circ)$  and  $R_2 = I_\gamma(133.6^\circ + 157.6^\circ)/I_\gamma(75.5^\circ)$ , thus providing two  $R$  values for each transition from which the final value was calculated as a weighted average (see Table I).

If allowed by the  $\gamma$ -ray intensity and cleanliness, two  $\beta$ -tagged (or  $\beta$ - and/or isomer tagged) singles  $\gamma$ -ray spectra corresponding to the sum of angles  $(133.6^\circ + 157.6^\circ)$  and  $(104.5^\circ + 75.5^\circ)$  with two different  $\beta$ -particle energy gates (large gate = 0.5–10 MeV and small gate = 3–10 MeV) were used to compute the  $R$  value. The resulting  $R$  values with error estimates for the  $^{66}\text{As}$   $\gamma$ -ray transitions are listed in Table I, where the method used is also indicated. Transitions of known multiplicities originating from nuclei populated via other reaction channels were analyzed with the methods described above, yielding, on average, angular distribution ratios of 1.30(7) for stretched  $\Delta I = 2$ ,  $E2$  and 0.70(6) for stretched  $\Delta I = 1$ ,  $M1$ , and  $E1$  type of transitions.

### III. RESULTS

The level scheme of  $^{66}\text{As}$  constructed in the present work is shown in Fig. 2. Details of the measured  $\gamma$ -ray transitions are listed in Tables I and II. These results are based on the prompt, delayed, and delayed-prompt  $\gamma\gamma$  coincidence analysis. Isomeric structures in  $^{66}\text{As}$  have been previously studied by Grzywacz *et al.*, leading to the discovery of two isomeric states and nine connecting  $\gamma$ -ray transitions [8]. Recently an

TABLE I. The prompt  $\gamma$ -ray transitions measured for  $^{66}\text{As}$ . The energy of the  $\gamma$  rays ( $E_\gamma$ ), relative  $\gamma$ -ray intensity ( $I_{\text{rel}}$ ) normalized to 100 for the  $2_1^+ \rightarrow 0_1^+$  transition, level energy ( $E_i$ ), assigned spin and parity of the initial and final levels ( $I_i^\pi$  and  $I_f^\pi$ ), and angular distribution information ( $A_2$  and  $R$ ) are listed.

| $E_\gamma$ (keV) | $I_{\text{rel}}$ (%) | $E_i$ (keV) | $I_i^\pi$    | $I_f^\pi$    | $A_2$    | $R$                   |
|------------------|----------------------|-------------|--------------|--------------|----------|-----------------------|
| 258.6(6)         | 15(1)                | 1600.3(9)   | (5)          | $3_2^+$      | 0.37(7)  | 1.56(13) <sup>a</sup> |
| 266.7(7)         | 5(2)                 | 1229.9(4)   | $3_1^+$      | $2_1^+$      |          | 0.69(18) <sup>b</sup> |
| 290.0(12)        | <10                  | 2478.6(6)   | $5_4^+$      | ( $4_3^+$ )  |          | 0.40(18) <sup>c</sup> |
| 354.6(5)         | 17(1)                | 2833.2(7)   | $7_2^+$      | $5_4^+$      | 0.23(11) | 1.46(14) <sup>a</sup> |
| 378.5(5)         | 31(2)                | 1341.7(6)   | $3_2^+$      | $2_1^+$      | -0.39(9) | 0.77(6) <sup>a</sup>  |
| 393.6(5)         | 28(1)                | 1229.9(4)   | $3_1^+$      | $1_1^+$      | 0.13(2)  | 1.22(9) <sup>a</sup>  |
| 506.0(11)        | 7(1)                 | 1341.7(6)   | $3_2^+$      | $1_1^+$      |          |                       |
| 521.1(8)         | 12(1)                | 1751.0(9)   | (4)          | $3_1^+$      |          | 1.29(25) <sup>d</sup> |
| 556.3(7)         | 19(1)                | 1519.3(8)   | (4)          | $2_1^+$      | 0.47(16) | 1.15(10) <sup>a</sup> |
| 669.7(6)         | 14(1)                | 1899.9(5)   | $5_3^+$      | $3_1^+$      | 0.59(20) | 1.33(28) <sup>b</sup> |
| 722.4(7)         | 15(4)                | 6530.4(11)  | ( $14_1^+$ ) | ( $12_1^+$ ) |          | 1.49(28) <sup>b</sup> |
| 727.7(7)         | 17(4)                | 2478.6(6)   | $5_4^+$      | (4)          |          | 0.60(14) <sup>b</sup> |
| 836.2(6)         | 42(3)                | 836.3(4)    | $1_1^+$      | $0_1^+$      | -0.36(3) | 0.70(12) <sup>e</sup> |
| 839.6(13)        | <10                  | 3673.6(12)  | ( $6_1^+$ )  | $7_2^+$      |          | 0.60(21) <sup>f</sup> |
| 840.9(5)         | 68(3)                | 3862.3(8)   | $11_1^+$     | $9_1^+$      | 0.30(5)  | 1.17(3) <sup>g</sup>  |
| 858.2(6)         | 11(3)                | 3691.4(10)  | ( $9_3^+$ )  | $7_2^+$      |          | 1.55(52) <sup>b</sup> |
| 902.2(6)         | 12(3)                | 3251.0(11)  | ( $9_2^+$ )  | ( $7_1^+$ )  |          | 1.35(23) <sup>i</sup> |
| 959.6(12)        | 24(8)                | 2478.6(6)   | $5_4^+$      | (4)          |          |                       |
| 962.8(5)         | 100(5)               | 963.0(4)    | $2_1^+$      | $0_1^+$      | 0.30(4)  | 1.27(15) <sup>j</sup> |
| 994.5(7)         | 18(3)                | 2348.8(9)   | ( $7_1^+$ )  | $5_1^+$      |          | 1.38(29) <sup>i</sup> |
| 1136.6(5)        | 22(4)                | 2478.6(6)   | $5_4^+$      | $3_2^+$      | 0.27(20) | 1.25(12) <sup>a</sup> |
| 1205.6(11)       | 18(2)                | 6530.4(11)  | ( $14_1^+$ ) | $13_1^+$     |          | 0.50(21) <sup>k</sup> |
| 1226.0(11)       | 6(1)                 | 2189.0(12)  | ( $4_3^+$ )  | $2_1^+$      |          | 1.64(58) <sup>l</sup> |
| 1262.0(11)       | 7(1)                 | 7792.4(16)  | ( $16_1^+$ ) | ( $14_1^+$ ) |          |                       |
| 1288.6(9)        | 8(3)                 | 2518.5(10)  | (4)          | $3_1^+$      |          | 0.45(24) <sup>d</sup> |
| 1462.3(6)        | 37(2)                | 5324.6(10)  | $13_1^+$     | $11_1^+$     | 0.51(7)  | 1.17(14) <sup>g</sup> |
| 1486.0(16)       | <3                   | 3673.6(12)  | ( $6_1^+$ )  | ( $4_3^+$ )  |          |                       |
| 1553.0(11)       | 5(1)                 | 2907.0(5)   | $7_3^+$      | $5_1^+$      |          |                       |
| 1946.0(11)       | 4(1)                 | 5808.3(14)  | ( $12_1^+$ ) | $11_1^+$     |          |                       |

<sup>a</sup>Summed  $\beta$ -tagged rings.

<sup>b</sup>Summed  $\beta$ -tagged rings with small  $\beta$  gate only.

<sup>c</sup>Gate on 355 and 840 keV.

<sup>d</sup>Gate on 394 and 836 keV.

<sup>e</sup>Gate on 394 and 670 keV.

<sup>f</sup>Gate on 290 and 355 keV.

<sup>g</sup>Summed recoil-isomer-tagged rings.

<sup>h</sup>Gate on 355 and 1137 keV.

<sup>i</sup>Summed recoil-isomer and  $\beta$ -tagged rings.

<sup>j</sup>Weighted average of gated (gate on 379 and 1137 keV) and summed  $\beta$ -tagged rings with 4.5- to 10-MeV  $\beta$ -gate.

<sup>k</sup>Gate on 841 and 1462 keV.

<sup>l</sup>Gate on 963 keV.

in-beam study performed by de Angelis *et al.* [10] provided information on several new  $\gamma$ -ray transitions bypassing the isomeric states. In the following, results from the present data concerning both the isomeric and the prompt structures are

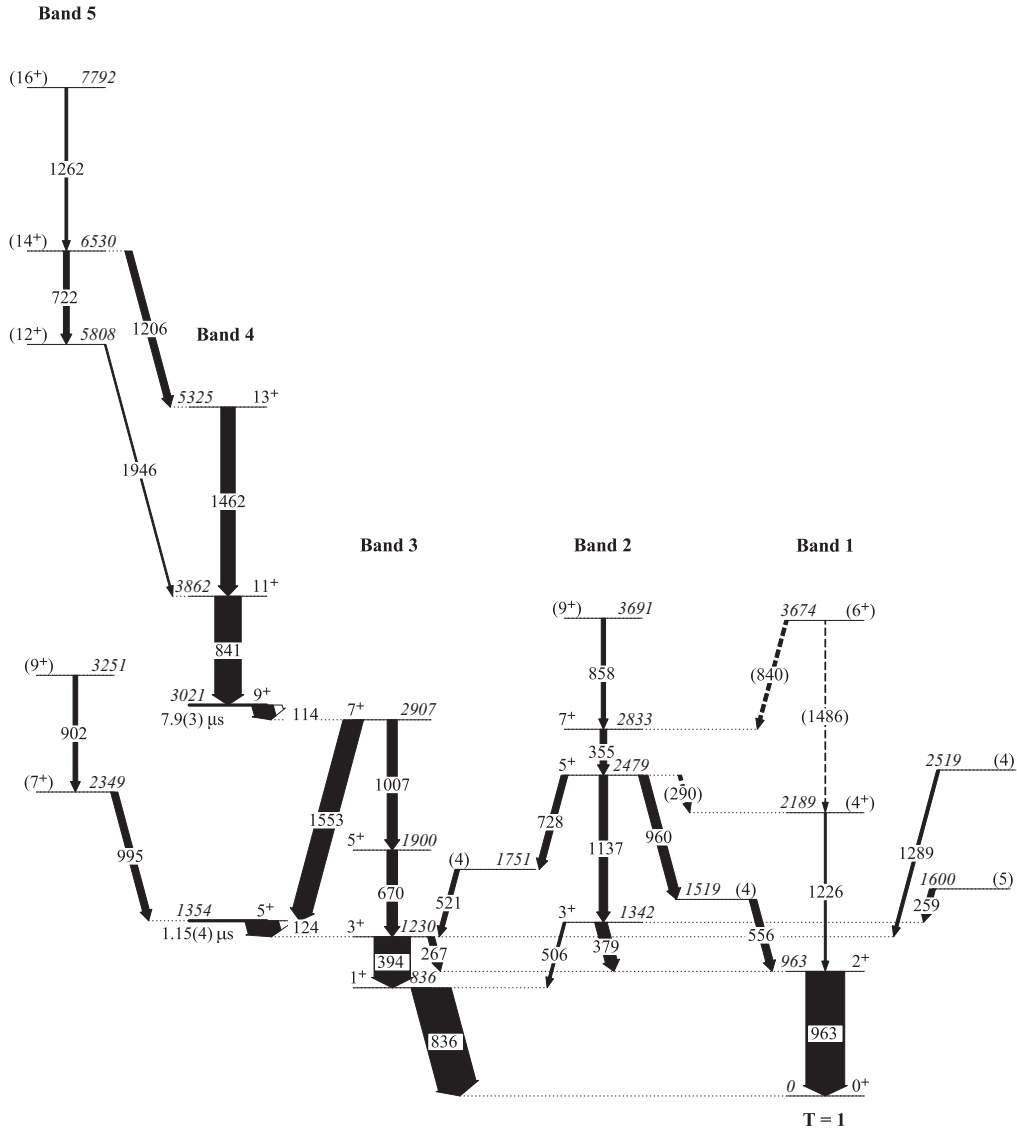


FIG. 2. Level scheme of  $^{66}\text{As}$  derived from the present data. The width of the arrow corresponds to the intensity of the transition extracted from  $\beta$ -tagged JUROGAM II singles data with 1- to 10-MeV  $\beta$  gate except for the delayed 114-, 124-, 267-, 394-, 670-, 836-, 1007-, and 1553-keV  $\gamma$ -ray transition intensities, which are obtained from  $\beta$ -tagged RITU focal plane data.

presented. A comparison to the previous works is carried out and discrepancies are discussed.

### A. Isomeric states in $^{66}\text{As}$

The delayed  $\gamma$ -ray transitions, which were identified in Ref. [8], were also observed in the present study. This is illustrated in Figs. 3(a) and 3(b) where the  $\beta$ -tagged delayed  $^{66}\text{As}$  singles  $\gamma$ -ray spectra recorded in the planar and GREAT clover detectors, respectively, are presented.

Coincidence relations between transitions below the isomeric states can be seen in Fig. 4, where  $\beta$ -tagged and gated  $\gamma$ -ray spectra from a planar-clover matrix are illustrated. The  $\gamma$  rays detected in the clover detector in coincidence with the 114-keV  $\gamma$  rays seen in the planar detector are shown in panel (a). Similarly, in panel (c)  $\gamma$  rays seen in the clover detector coinciding with the  $\gamma$  rays at 124 keV seen in the planar detector are presented. In panels (b) and (d) the same

data are illustrated as in panels (a) and (c) but there is now a narrow  $\gamma\gamma$  time gate of  $-100$ – $100$  ns added to identify only prompt coincidences. The time gate on the  $\gamma_{\text{planar}}$ -recoil time difference was set to  $0$ – $21$   $\mu\text{s}$  ( $\approx 3 \times t_{1/2}^{114\text{keV}}$ ) in all panels of Fig. 4. A comparison between panels (a) and (b) immediately reveals that the 124-keV transition is directly depopulating one of the isomeric states as the line at 124 keV disappears when imposing the prompt coincidence time gate. All of the other seven  $\gamma$ -ray peaks still remain in prompt coincidence with the 114-keV line when the  $\gamma\gamma$  time gate is applied, indicating that the 114-keV transition is directly deexciting the other isomeric state. Comparing panels (c) and (d) confirms the conclusions made above since the 124-keV line is no longer seen in coincidence with the 114- and 1553-keV lines after the narrow  $\gamma\gamma$  time gate is added. In addition, the isomeric state depopulated by the 124-keV line has to lie lower in excitation energy as it is fed from above by the 1553-keV  $\gamma$ -ray

TABLE II. The  $\gamma$  rays measured for  $^{66}\text{As}$  at the focal plane of RITU. Intensities are relative to the  $1_1^+ \rightarrow 0_1^+$  836-keV transition.

| $E_\gamma$ (keV) | $I_{\text{rel}}$ (%) | $E_i$ (keV) | $I_i^\pi$ | $I_f^\pi$ | $\alpha_{\text{tot}}$ | $t_{1/2}$ ( $\mu\text{s}$ ) |
|------------------|----------------------|-------------|-----------|-----------|-----------------------|-----------------------------|
| 114.4(2)         | 54(4)                | 3021.4(6)   | $9_1^+$   | $7_3^+$   | 0.41(13)              | 7.9(3)                      |
| 124.4(2)         | 84(2)                | 1354.3(5)   | $5_1^+$   | $3_1^+$   | 0.31(16)              | 1.15(4)                     |
| 267.1(3)         | 17(5)                | 1229.9(4)   | $3_1^+$   | $2_1^+$   |                       |                             |
| 393.6(3)         | 93(4)                | 1229.9(4)   | $3_1^+$   | $1_1^+$   |                       |                             |
| 670.1(5)         | 27(3)                | 1899.9(5)   | $5_3^+$   | $3_1^+$   |                       |                             |
| 836.3(4)         | 100(6)               | 836.3(4)    | $1_1^+$   | $0_1^+$   |                       |                             |
| 963.1(5)         | 17(3)                | 963.0(4)    | $2_1^+$   | $0_1^+$   |                       |                             |
| 1006.7(5)        | 26(3)                | 2907.0(5)   | $7_3^+$   | $5_3^+$   |                       |                             |
| 1553.0(4)        | 51(4)                | 2907.0(5)   | $7_3^+$   | $5_1^+$   |                       |                             |

transition. The ordering of the 114- and 124-keV transitions was further confirmed by comparing the time stamps of these decay events. This was possible due to the time stamping with 10-ns precision of each data event in the TDR system. A comparison of the time stamps for the 114- and 124-keV  $\gamma\gamma$  coincidences leads to the conclusion that in 98% of the detected coincidences, the 114-keV transition precedes the 124-keV transition.

The 1007- and 670-keV  $\gamma$ -ray transitions are seen in coincidence only with the 114-keV  $\gamma$ -ray transition, which indicates that they bypass the lower-lying isomeric state. However, the 1553-keV line is seen in coincidence with both the 114- and 124-keV lines and, as stated earlier, the 1553-keV transition precedes the 124-keV transition, as does the 114-keV transition. This leads to the conclusion that the isomeric states are connected by the consecutive 114- and 1553-keV  $\gamma$  rays. The sum of energies of the 124- and 1553-keV  $\gamma$ -ray transitions equals the sum of the 670- and 1007-keV transitions, which are concluded to form a parallel cascade with the 124- and 1553-keV transitions. When imposing the narrow  $\gamma\gamma$  time gate on the spectrum gated by the 124-keV  $\gamma$ -ray transition, coincidences are only observed with the 267-, 394-, 836-, and 963-keV transitions as illustrated in Fig. 4(d). This stems from the fact that the previously mentioned transitions must originate from states lying below the lower-lying isomeric state.

Recoil-gated spectra from the planar-clover matrix are presented in Fig. 5 showing  $\gamma$ -ray transitions observed in the clover detector in coincidence with the 394- and 267-keV transitions detected in the planar. The reduction in statistics from  $\beta$ -tagging added to the drop in  $\gamma$ -ray detection efficiency of the planar detector above 150 keV did not permit a  $\beta$ -tagged  $\gamma\gamma$  analysis for these transitions. Observed coincidences presented in Fig. 5 show that the 670-, 836-, and 1007-keV  $\gamma$ -ray transitions are in coincidence with the 394-keV transition and that the 670-, 963-, and 1007-keV transitions are in coincidence with the 267-keV transition. As the 267- and 394-keV lines are not seen in mutual coincidence and the sum of energies of the 267- and 963-keV transitions equals the sum of the 394- and 836-keV transitions, it can be concluded that they form parallel cascades depopulating a state at 1230 keV. This state is fed by the 670-keV/1007-keV cascade from a state at 2907 keV. The ordering of the  $\gamma$ -ray transition pairs

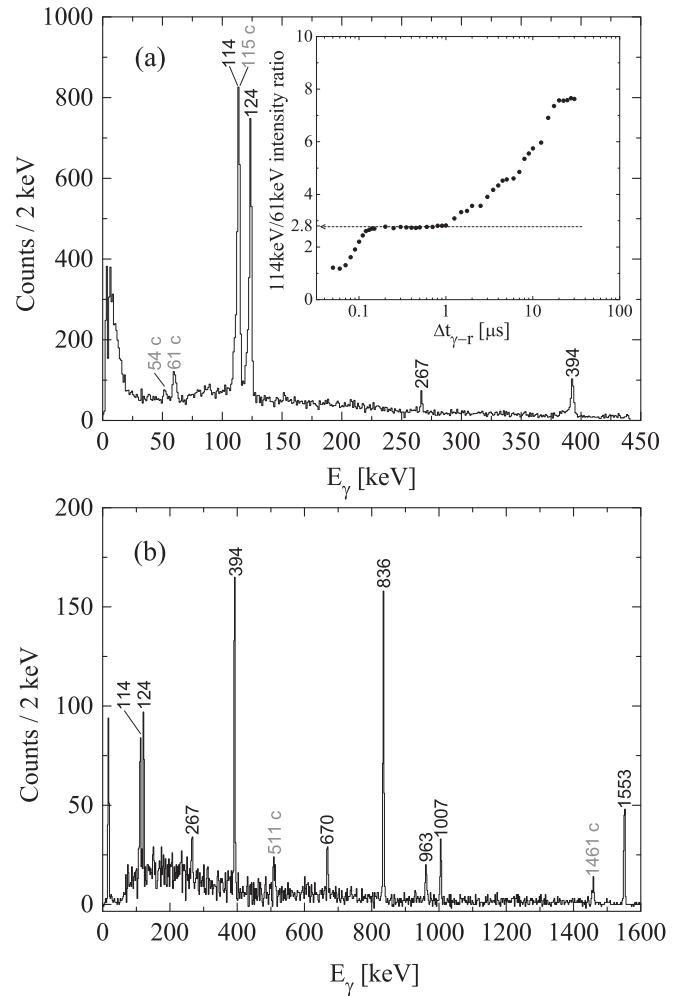


FIG. 3.  $\beta$ -tagged delayed  $^{66}\text{As}$   $\gamma$  rays detected in the (a) planar and (b) clover germanium detectors. The low-energy threshold for the  $\beta$  particles was set to 1 MeV. Transitions with gray labels (and marked with a “c”) in panel (a) are contaminants from the  $^{65}\text{Ga}$   $\beta$  decay feeding the excited states of  $^{65}\text{Zn}$ . The time gate for  $\gamma$ -recoil time difference is 0–21  $\mu\text{s}$ . Inset in panel (a): The intensity ratio of  $\beta$ -tagged 114- and 61-keV  $\gamma$  rays observed in the planar detector as a function of  $\gamma$ -recoil time difference. Information on the  $^{65}\text{Ga}$  contamination in the  $^{66}\text{As}$  114-keV peak can be obtained from the flat part of the curve (see Sec. III A2 for details).

with energies of 670 keV/1007 keV, 394 keV/836 keV, and 267 keV/963 keV cannot be assigned unambiguously at this stage. This is established later on by prompt  $\gamma\gamma$  analysis (see Secs. III B1 and III B2).

### 1. Half-lives of the isomeric states

Half-lives of the isomeric states were determined making use of the logarithmic binning method described by Schmidt *et al.* [30,31]. This method is very convenient for discriminating between different radioactive species and is applicable especially in the cases where only limited statistics are available. In this method, the number of radioactive decay events are plotted against the natural logarithm of the time differences giving rise to a bell-shaped distribution. The

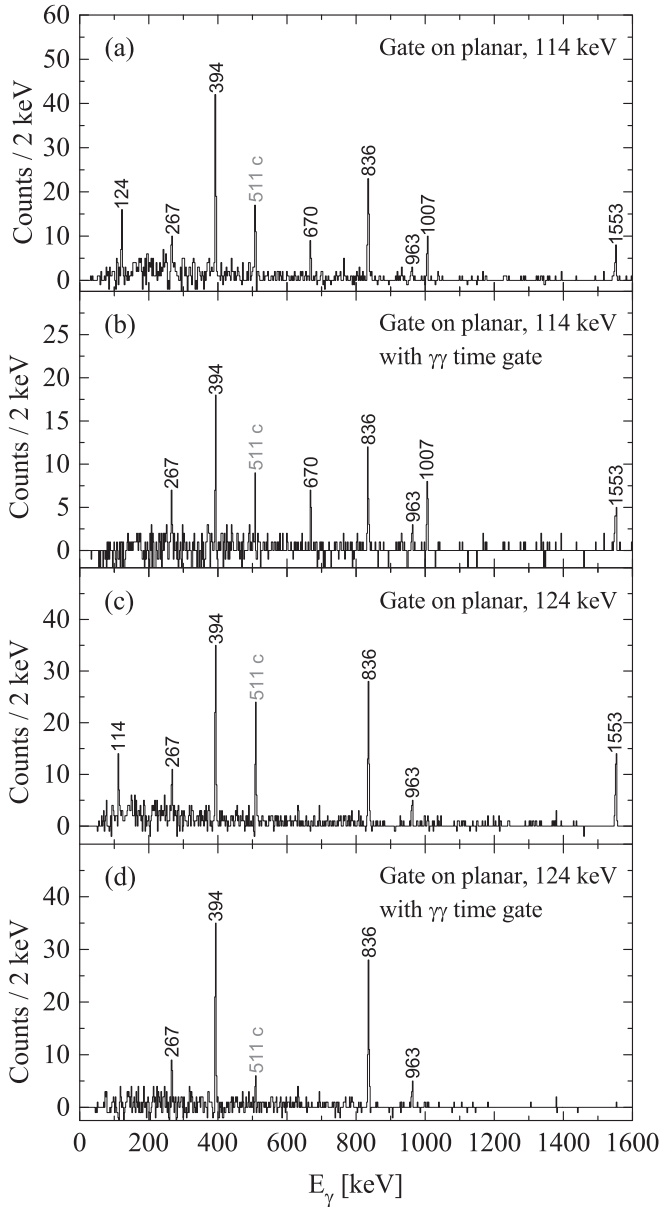


FIG. 4.  $\beta$ -tagged and gated delayed  $\gamma$ -ray spectra from planar-clover matrices. In panels (a) and (b) the gate is set on the 114-keV transition detected in planar, whereas in panels (c) and (d) the gate is set on the 124-keV transition. In all panels the  $\beta$  gate was set to 0.5–10 MeV and  $\gamma_{\text{planar}}$ -recoil time gate to 0–21  $\mu\text{s}$ . Panels (b) and (d) have a narrow –100- to 100-ns  $\gamma\gamma$  time gate applied to identify only prompt  $\gamma$ -ray coincidences.

half-life can be extracted from the centroid of this distribution. The two-component function fitted to the half-life data is of the form

$$\left| \frac{dn}{d\Theta} \right| = (n_1 \lambda_1 e^{-\lambda_1 \Theta} + n_2 \lambda_2 e^{-\lambda_2 \Theta}) e^{-\Theta}, \quad (1)$$

where a substitution  $\Theta = \ln t$  is introduced,  $n_i$  and  $\lambda_i$ , where  $i = \{1, 2\}$  are the number of counts and decay constants of two different activities, respectively. Figure 6 presents the half-life data and the fitted two-component functions under various gating conditions. The black and red data points

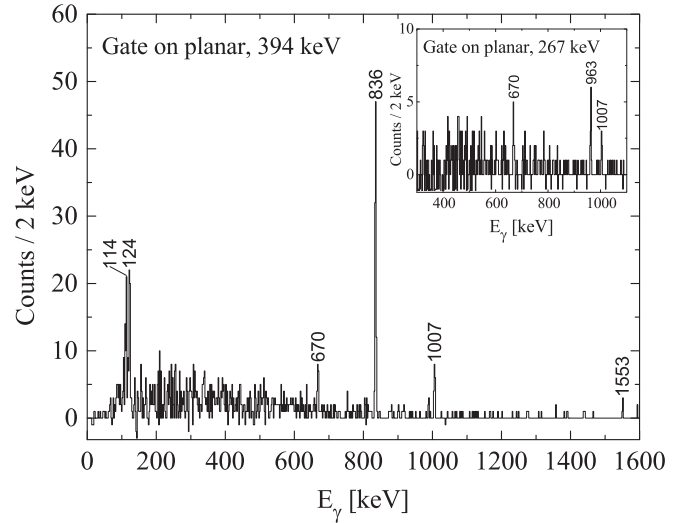


FIG. 5. Recoil-gated delayed  $\gamma$  rays from the planar-clover matrix. The gate is set on the 394-keV transition detected in the planar, whereas in the inset the gate is set on the 267-keV transition. The time gate for  $\gamma_{\text{planar}}$ -recoil time difference is set to 0–21  $\mu\text{s}$  in the main figure and to 0–5  $\mu\text{s}$  in the inset in order to avoid random coincidences with contaminant  $\gamma$  rays. In addition, a narrow –100- to 100-ns  $\gamma\gamma$  time gate is applied in both panels.

correspond to recoil-correlated and  $\beta$ -tagged delayed  $\gamma$ -ray data, respectively. The solid curves represent fits of Eq. (1) to the data. Recoil-gated data provide the desired statistics for reliable half-life determinations but to verify the accuracy of the results, the  $\beta$ -tagging conditions were also applied. The larger peaks in the time distributions presented in Figs. 6(a) and 6(b) correspond to real activities caused by the decay of the isomeric states, whereas the smaller components at higher  $\ln(\Delta t)$  values are attributable to random background. In the case of the higher-lying isomeric state, the half-life can be extracted from  $\gamma$ -recoil time differences of the 1553-keV  $\gamma$  rays detected in the GREAT clover detector. Other  $\gamma$  rays such as the 1007- and 670-keV transitions below the higher-lying isomeric state could have been used. However, this causes the random component to become the dominant part of the distribution owing to the background at lower energies originating mainly from Compton scattering. Using a single  $\gamma$ -ray energy gate to extract reliable  $\gamma$ -recoil time differences for the lower-lying isomeric state does not work owing to feeding of the higher-lying isomer. To overcome this issue, the time difference of two or more  $\gamma$  rays detected in the planar and clover detectors can be resolved. The time-difference spectrum presented in Fig. 6(b) shows the time difference between the 114- or 1553-keV transition recorded in the clover detector and the 124-keV transition observed in the planar detector. This method provides a low background time distribution in both recoil-correlated and  $\beta$ -tagged cases to accurately determine the half-life of the lower-lying isomeric state. An extremely clean time distribution can be obtained using the  $\beta$ -tagging condition without any random background events for the lower-lying isomeric state by excluding the detection of the 114-keV  $\gamma$  ray in the clover from the gating conditions, but naturally this yields fewer statistics. The time distribution

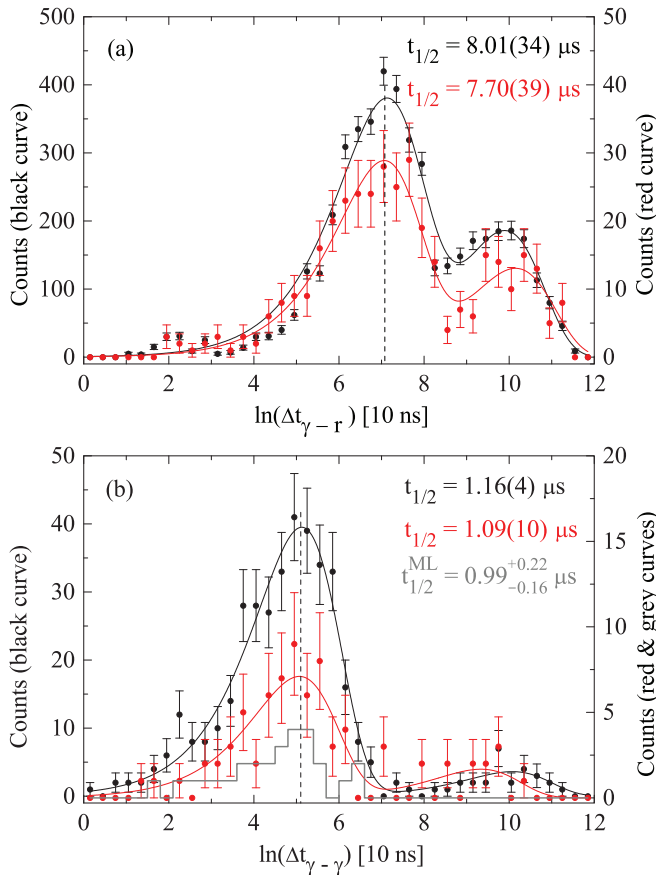


FIG. 6. (Color online) Half-life data and fits used to extract the half-lives of the (a) 3021-keV and (b) 1354-keV isomeric states, respectively. The dashed line indicates the centroid of the time distribution, which corresponds to the half-life of the state. Details of the time spectra and determination of the half-lives are explained in the text.

obtained in this way is shown in Fig. 6(b) as a gray histogram. The half-life is extracted from the data by using the maximum likelihood method [30].

Half-lives for the  $^{66}\text{As}$  isomeric states can be extracted from the fitted  $\lambda_1$  parameter which yields  $t_{1/2} = 8.01(34) \mu\text{s}$  from the recoil-correlated data and  $t_{1/2} = 7.70(39) \mu\text{s}$  from the  $\beta$ -tagged data for the higher-lying isomeric state. Corresponding values for the lower-lying isomeric state are  $t_{1/2} = 1.16(4) \mu\text{s}$  from the recoil-correlated data and  $t_{1/2} = 1.09(10) \mu\text{s}$  from the  $\beta$ -tagged data. Applying the maximum likelihood method to the data, presented in Fig. 6(b) as a gray histogram, produces a value of  $t_{1/2} = 0.99^{+0.22}_{-0.16} \mu\text{s}$  for the lower-lying state. The values obtained from differently conditioned data are consistent within error limits and can be considered to give accurate values for the isomeric half-lives. To combine the final values for the half-lives, a weighted average was calculated for each isomer, yielding  $t_{1/2} = 7.9(3) \mu\text{s}$  and  $t_{1/2} = 1.15(4) \mu\text{s}$  for the higher- and lower-lying isomeric states, respectively. These values and the ones reported in Ref. [9] are in agreement within error limits.

In the present study data were also produced for the  $^{69}\text{Ge}$  and  $^{65}\text{Zn}$  nuclei, which both contain long-lived states.

Previously reported half-lives for the  $9/2^+$  state at 398 keV in  $^{69}\text{Ge}$  are 2.79(6), 2.84(7), and 3.2(6)  $\mu\text{s}$  [32]. The ones for the  $(1/2)^-$  state at 54 keV in  $^{65}\text{Zn}$  are 1.52(9) and 1.65(5)  $\mu\text{s}$  [33]. The recorded delayed  $\gamma$  rays originating from  $^{69}\text{Ge}$  and  $^{65}\text{Zn}$  provide a perfect test for the validity of the half-life determination method described above. Similar analysis as carried out for the  $^{66}\text{As}$  yields half-life values of 2.70(8)  $\mu\text{s}$  for the  $9/2^+$  state in  $^{69}\text{Ge}$  and 1.51(7)  $\mu\text{s}$  for the  $(1/2)^-$  state in  $^{65}\text{Zn}$ . These values are in agreement within error limits with the weighted averages of the previously reported values [2.81(5)  $\mu\text{s}$  for  $^{69}\text{Ge}$  and 1.62(6)  $\mu\text{s}$  for  $^{65}\text{Zn}$ ].

## 2. Internal conversion coefficients of the isomeric $\gamma$ -ray transitions

The total internal conversion coefficients can be determined for the two transitions deexciting the isomeric states by demanding the preservation of the  $\gamma$ -ray intensity through a cascade. To evaluate the intensity balance, detailed information on the detector efficiencies is crucial. Efficiency curves for the planar and the clover germanium detectors were simulated with a GEANT4 toolkit [34] according to the experimental circumstances. The distribution of implanted recoils in the DSSD and the thickness of the implantation detector were taken into account in these simulations. As RITU is designed to operate in heavier mass region, the separation of fusion residues from the primary beam and other unwanted products is challenging in the mass  $A = 70$  region. For this reason, the optimal settings for RITU could not be used, which caused the recoil distribution to be focused more on the right-hand side of the DSSDs. Clearly, if the recoil distribution is not uniform across the DSSD, the  $\gamma$ -ray detection efficiencies of the planar and clover detectors placed around the DSSD will be affected by this geometrical deviation.

The total intensity of the 114-keV transition feeding a state, which is depopulated by the 1007- and 1553-keV transitions, has to equal the sum of the intensities of the latter mentioned transitions. The internal conversion of the 1007- and 1553-keV transitions is negligible owing to the high energies, so there is no need to make assumptions about the transition characteristics nor correct the experimental intensities for conversion. The efficiency-corrected intensity of the  $\beta$ -tagged 114-keV  $\gamma$ -ray transition observed in the planar is thus compared to the sum of the efficiency-corrected intensities of the  $\beta$ -tagged 1007- and 1553-keV  $\gamma$  rays detected in the clover to resolve the total internal conversion coefficient for the 114-keV transition. Despite the  $\beta$ -tagging conditions, there is always a certain amount of contaminant events in the 114-keV planar peak originating from random correlations of the  $^{65}\text{Ga}$   $\beta$  decay to the excited states in  $^{65}\text{Zn}$ , where one of the states is depopulated by a 115-keV  $\gamma$ -ray transition. Fortunately, the magnitude of contamination can be estimated and corrected for, as there is also a 61-keV  $\gamma$ -ray transition depopulating the same state as the 115-keV transition in  $^{65}\text{Zn}$ . The intensity ratio of these transitions can be resolved as a function of  $\gamma$ -recoil time differences in order to obtain a correction factor for the 114-keV  $\gamma$ -ray intensity. This is shown in Fig. 3(a) as an inset. At time differences between 0.1 and 1  $\mu\text{s}$ , the intensity ratio of the 114- and 61-keV

peaks remains at a constant value, as it should before the ratio starts to increase monotonically owing to the decay of the higher-lying isomeric state in  $^{66}\text{As}$ , which increases the intensity of the 114-keV peak rapidly. The correction factor 2.8 can be obtained from the plateau in the curve, which is then used to subtract the intensity corresponding to the contamination ( $2.8 \times I_{61\text{keV}}$ ) from the total intensity of the 114-keV peak. After this correction, the total internal conversion coefficient can be determined, yielding the value of  $\alpha_{\text{exp}} = 0.41(13)$  for the 114-keV transition in  $^{66}\text{As}$ . The closest total internal conversion coefficients for this transition energy obtained from Ref. [35] are  $\alpha_{\text{th}}^{E2} = 0.48(1)$  and  $\alpha_{\text{th}}^{M2} = 0.59(1)$ , hence suggesting the transition has an  $E2$  character. The error of the theoretical value originates from the uncertainty in the energy measurement of the 114-keV  $\gamma$  ray.

The total intensity of the 124-keV transition has to equal the sum of the 267- and 394-keV transition intensities as they feed and deexcite the same state. The problem is that this state is also fed from the higher-lying isomer via the 1007- and 670-keV transitions. As there is a large difference between the isomeric half-lives, setting a strict 0- to 1- $\mu\text{s}$  time gate on the  $\gamma$ -recoil time difference, the additional feeding from above can be eliminated. The validity of the time gate can be verified from the plot presented in the inset of Fig. 3(a). Theoretical total internal conversion coefficients for the 267- and 394-keV transitions are practically negligible for any of the multiplicities below  $\lambda = 4$ . Therefore, no assumptions on their character are needed nor corrections to the intensity for conversion. The efficiency-corrected intensity of the  $\beta$ -tagged 124-keV transition detected in the planar is thus compared to the sum of the efficiency-corrected intensities of the  $\beta$ -tagged 267- and 394-keV transitions detected also in the planar giving rise to the total internal conversion coefficient of  $\alpha_{\text{exp}} = 0.31(16)$ . Relevant coefficients obtained from Ref. [35] are  $\alpha_{\text{th}}^{E2} = 0.35(1)$  and  $\alpha_{\text{th}}^{M2} = 0.43(1)$ , confirming the 124-keV transition multipolarity to be  $\lambda = 2$  and suggesting an electric character.

The experimental conversion coefficients reported in Ref. [8] are 1.3(4) for the 114-keV transition and 0.7(3) for the 124-keV transition. The discrepancies probably result from the underestimation of the  $\gamma$ -ray intensities in Ref. [8] owing to a large Compton background.

### B. Short-lived states in $^{66}\text{As}$

The  $\gamma$  rays originating from  $^{66}\text{As}$  can be identified already with a large 1- to 10-MeV  $\beta$  gate, as illustrated in Fig. 7(a). This is essential when statistics are needed for the  $\gamma\gamma$  analysis and angular distributions. However, the spectrum tagged with the majority of detected  $\beta$  particles suffers from heavy contamination caused by stronger reaction channels such as  $^{66}\text{Ge}$  and  $^{65}\text{Ga}$ , which were the main contaminants. Raising the  $\beta$ -particle detection threshold by 2 MeV allows for clean identification of  $^{66}\text{As}$   $\gamma$  rays. From the  $\beta$ -tagged singles spectrum shown in Fig. 7(b), five prominent peaks located at energies of 355, 379, 394, 836–841, and 960–963 keV can be observed. These transitions have to originate from levels rather close to the ground state of  $^{66}\text{As}$  because one would expect a rapid increase in the level density, hence strong

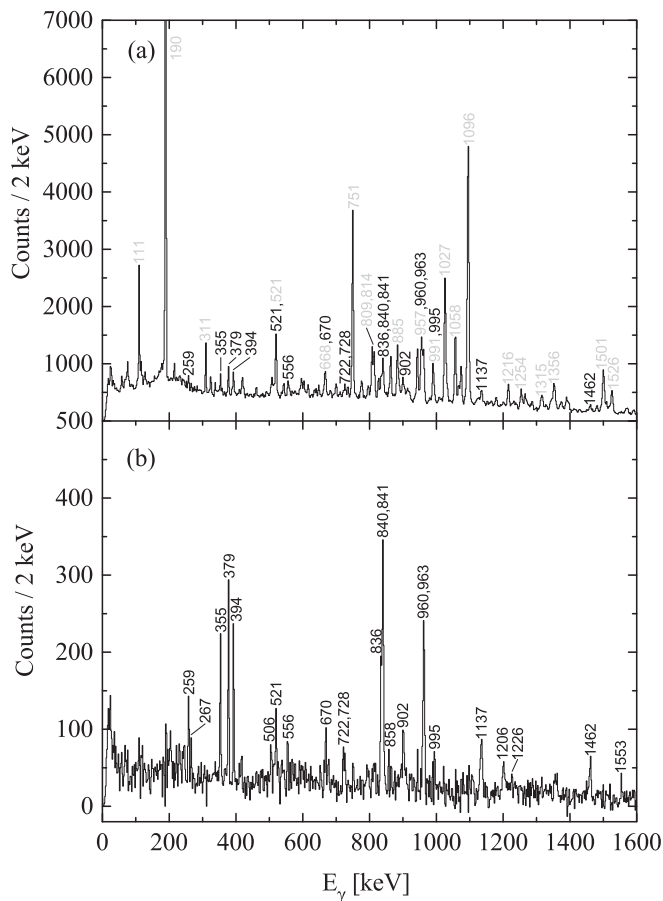


FIG. 7. Recoil  $\beta$ -tagged JUROGAM II singles spectra with a 300-ms correlation time. In panel (a) the  $\beta$ -particle energy gate is set at 1–10 MeV, whereas in panel (b) it is set at 3–10 MeV, with a background subtraction condition added to eliminate randomly correlated  $\gamma$ -ray transitions. Peaks labeled in black are transitions associated with  $^{66}\text{As}$ , while gray labels are for transitions originating from other reaction channels such as  $^{66}\text{Ge}$ ,  $^{65}\text{Ge}$ ,  $^{65}\text{Ga}$ , and  $^{64}\text{Zn}$ .

fragmentation of the  $\gamma$ -ray transition intensity, when going to higher excitation energy. The prominent peaks listed represent decays from both the  $T = 0$  and the  $T = 1$  states in  $^{66}\text{As}$ . In the following discussion the results concerning the prompt  $\gamma$ -ray transitions are presented. The experimentally observed excited states in  $^{66}\text{As}$  have been divided into isospin  $T = 1$  and  $T = 0$  structures. The illustrated  $\gamma\gamma$  coincidence spectra represent cases where rather strict  $\beta$  gates ( $\sim 3$ –10 MeV) have been used to show the cleanest coincidences. This naturally excludes some of the good events, which are more pronounced with relaxed gating conditions along with the contaminant  $\gamma$ -ray transitions. Coincidence spectra illustrated in Figs. 8(a) and 8(b) represents the effect of the size of the  $\beta$  gate on the observed coincidences. In panel (b), the low-energy threshold is raised by 1.5 MeV, which produces a clean and low-background spectrum but the coincidence with the 1137-keV transition seems to be missing although it can be clearly identified in panel (a). In the other spectra shown in Figs. 9 and 10, all the transitions which have been found to coincide with the gating transition with relaxed tagging

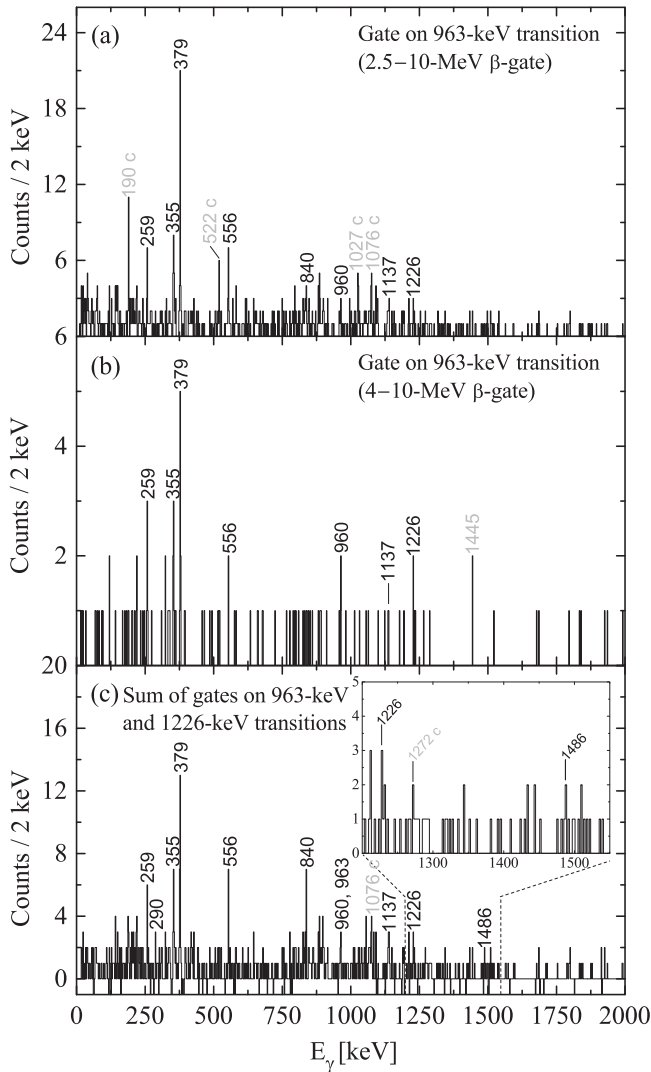


FIG. 8.  $\beta$ -tagged and gated prompt JUROGAM II spectra illustrating observed coincidences within the  $T = 1$  band and between  $T = 0$  and  $T = 1$  bands. In panels (a) and (b) the gate is set on the 963-keV transition with  $\beta$ -particle energy gates of 2.5–10 and 4–10 MeV, respectively, to illustrate the effect of the size of the  $\beta$  gate on the gated spectra. In panel (c) the gates are set on the 963- and 1226-keV transitions with a 2.5- to 10-MeV  $\beta$  gate. The inset shows the low-background region where the 1226- and 1486-keV lines are identified. In each panel background subtraction is performed by setting a background gate, which has the same width as the main gate, near the gating transition. Peaks labeled in gray and marked with a “c” are contaminants from  $^{66}\text{Ge}$ ,  $^{65}\text{Ga}$ , and  $^{64}\text{Zn}$ .

conditions are labeled even if they do not clearly stand out from the background in these particular figures.

### 1. $T = 1$ states

The ground state of  $^{66}\text{As}$  is expected to be  $T = 1$ ,  $I^\pi = 0^+$  [8–10,36], which is known to  $\beta$  decay to the  $T = 1$ ,  $0^+$  ground state of  $^{66}\text{Ge}$  via a Fermi superallowed transition [25–28]. Taking into account the isospin symmetry between isobaric multiplets, the closest transition in  $^{66}\text{As}$ , energywise, to the  $^{66}\text{Ge } 2_1^+ \rightarrow 0_1^+$  transition is the 963-keV transition [37].

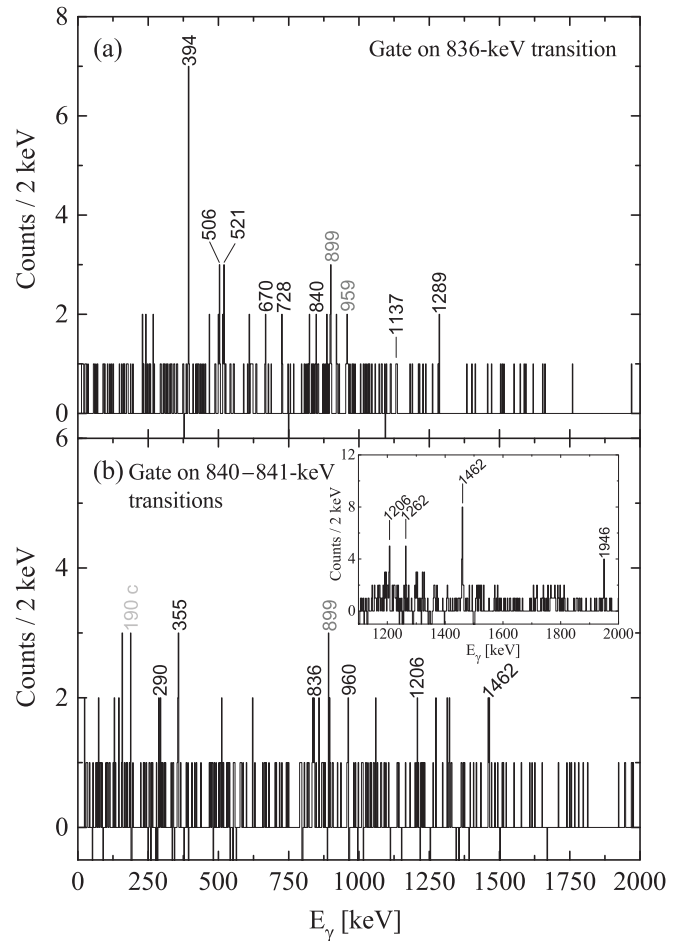


FIG. 9.  $\beta$ -tagged and gated prompt JUROGAM II coincidence spectra. In panel (a) the gate is set on the 836-keV transition with 2.75- to 10-MeV  $\beta$  gate. In panel (b) the gate is set on the 840- to 841-keV transitions with 3.25- to 10-MeV  $\beta$  gate. The inset in panel (b) illustrates a part of the coincidence spectrum gated by the 840- to 841-keV transitions with 1.5- to 10-MeV  $\beta$  gate. Peaks labeled in dark gray are unidentified transitions while the one labeled in gray and marked with a “c” is a contaminant from  $^{65}\text{Ga}$ .

The angular distribution information [ $A_2 = 0.30(4)$ ] and the value of the angular distribution ratio [ $R = 1.27(15)$ ] obtained for the 963-keV peak suggests a stretched  $E2$  character. Thus, on the basis of intensity and energy arguments, the 963-keV transition is assigned as the  $2_1^+ \rightarrow 0_1^+$  transition in  $^{66}\text{As}$ . Analysis of the  $\gamma\gamma$  coincidences, with a gate set on the 963-keV transition and simultaneously varying the size of the  $\beta$  gate, reveals a peak located at 1226 keV (see Fig. 8). When the gate is set on the 1226-keV transition, the most intense coincidence is seen with the 963-keV transition; thus, these two transitions can be concluded to form a cascade. The energy of the  $4_1^+ \rightarrow 2_1^+$  transition found in  $^{66}\text{Ge}$  is 1216 keV, which is rather close to 1226 keV. These arguments along with the deduced angular distribution ratio of  $R = 1.64(58)$  for the 1226-keV transition suggests that it is the second transition in the  $^{66}\text{As } T = 1$  band deexciting a  $4_3^+$  state at 2189 keV. Further investigation of the coincidence events gated by the 1226-keV transition reveals a  $\gamma$ -ray peak at an energy of

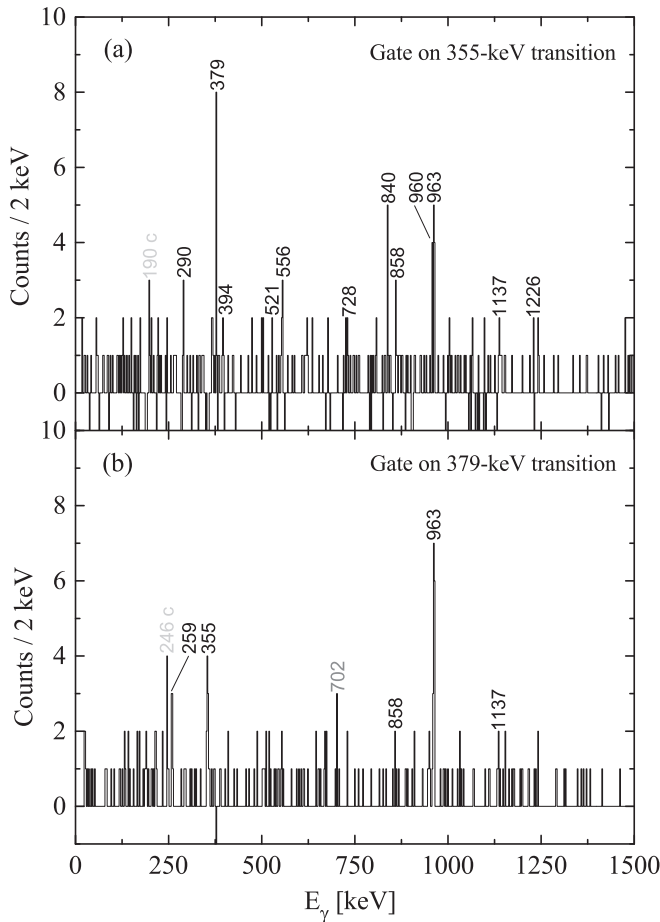


FIG. 10.  $\beta$ -tagged and gated prompt JUROGAM II spectra with gate on the (a) 355-keV and (b) 379-keV  $\gamma$ -ray transitions. The size of the  $\beta$  gate is 3.25–10 MeV in the both panels. Peaks labeled in gray and marked with a “c” are contaminants from  $^{65}\text{Ga}$  and  $^{62}\text{Ga}$ , while the one labeled in dark gray is an unidentified transition.

1486 keV. This transition stands out from the background with a rather large  $\beta$  gate of the order of 2–10 MeV and it can be distinguished as a separate peak from the  $^{66}\text{Ge}$   $6_1^+ \rightarrow 4_1^+$  1481-keV transition. The 1486-keV transition is tentatively assigned to deexcite the  $T = 1$ ,  $6_1^+$  state at 3674 keV, because of the similarity with the corresponding transition found from  $^{66}\text{Ge}$  and observed coincidence relations. Coincident events with the 963- and 1226-keV lines are illustrated in Fig. 8(c), where the low-background region containing the candidates for the  $4_3^+ \rightarrow 2_1^+$  and  $6_1^+ \rightarrow 4_3^+$  transitions is shown in the inset. The peak at 1272 keV is a contaminant from  $^{64}\text{Zn}$ . Further proof for the existence of the level at 3674 keV can be obtained from the other observed coincidences as discussed in Sec. III B3.

## 2. $T = 0$ states

The 836-keV transition seen in both delayed and prompt spectra is assigned to deexcite the lowest  $T = 0$ ,  $1_1^+$  level. This fact is supported by the observed high intensity of prompt  $\gamma$  rays and the conclusions made from the delayed coincidence data. Furthermore, both the extracted angular distribution

coefficient [ $A_2 = -0.36(3)$ ] and the value of angular distribution ratio [ $R = 0.70(12)$ ] are indicative of a stretched  $\Delta I = 1$ ,  $M1$  transition. The prompt coincidences seen with a gate on the 836-keV transition are shown in Fig. 9(a). The most intense coincidences, when the  $\beta$  gate is relaxed slightly, occur with the 394- and 670-keV transitions. Both of these transitions were also seen in the delayed spectra; thus it can be assumed that these three transitions form a  $T = 0$  cascade (Band 3). Angular distribution information obtained for the 394- and 670-keV lines suggests that they are both stretched  $\Delta I = 2$ ,  $E2$  transitions. Taking into account the  $\gamma$ -ray intensities deduced from the delayed data (see Table II), the 394- and 670-keV transitions are assigned to deexcite a  $3_1^+$  state at 1230 keV and a  $5_3^+$  state at 1900 keV, respectively. It was confirmed earlier that the isomeric 124-keV  $\gamma$ -ray transition, with experimental conversion coefficient corresponding to an  $E2$  character, is feeding the state at 1230 keV. Therefore, the isomeric state at 1354 keV is assigned as  $5_1^+$ . The nonobservation of the 1007-keV transition, which clearly belongs to the same  $T = 0$  cascade with the 836-, 394-, and 670-keV transitions, in the prompt data might be attributable to the nonyrast nature of the 1553-keV transition, which deexcites the same state. Remembering the experimental conversion coefficient, which suggests  $E2$  character for the isomeric 114-keV  $\gamma$ -ray transition feeding the state at 2907 keV, the states at 2907 and 3021 keV can be assigned as  $7_3^+$  and  $9_1^+$ , respectively.

The most intense coincidence with the 963-keV transition appears to be the 379-keV line, as illustrated in Fig. 8; hence, the 379-keV transition is concluded to feed the  $2_1^+$  state at 963 keV from another  $T = 0$  sequence. The angular distribution coefficient [ $A_2 = -0.39(9)$ ] and the angular distribution ratio [ $R = 0.77(6)$ ] obtained for the 379-keV transition strongly imply a stretched  $\Delta I = 1$ ,  $M1$  character for this  $\gamma$  ray; therefore, a spin assignment of  $3_2^+$  is made for the  $T = 0$  level at 1342 keV. The 379- and 355-keV transitions are seen in strong mutual coincidence. The 355-keV line is seen also in coincidence with the 728-, 521-, and 394-keV mutually coinciding transitions, which in turn are seen from below by the  $1_1^+ \rightarrow 0_1^+$  836-keV transition. This supports the fact that the 1137-keV transition lies between the 355- and 379-keV transitions. Both of these  $\gamma$ -ray transitions naturally see the 1137-keV line, as can be noted from Figs. 10(a) and 10(b). The 379-, 1137-, and 355-keV transitions are concluded to belong to the same  $T = 0$  band (Band 2). The angular distribution coefficients and ratios suggest  $E2$  character for both the 1137- and the 355-keV transitions. Therefore, spin assignments of  $5_4^+$  and  $7_2^+$  are made for the  $T = 0$  levels at 2479 and 2833 keV, respectively. It should be noted that the  $\gamma$ -ray energies of the parallel branches consisting of the transitions of 963, 379, and 1137 keV and 836, 394, 521, and 728 keV add to the same sum energy of 2479 keV. The angular distribution ratio obtained for the 728-keV transition partially deexciting the  $5_4^+$  level at 2479 keV has a value expected from an  $M1$  character, whereas the  $R$  value of the subsequent 521-keV transition is consistent with a mixed  $M1/E2$  transition. Based on these numbers, the level at 1751 keV is tentatively assigned as  $I = 4$ .

The 556-keV transition is seen in coincidence with the 355- and 963-keV transitions, where the coincidence with

the latter  $\gamma$  ray seems to be more intense. For this reason the 556-keV transition is assigned to feed the  $2_1^+$  state at 963 keV from a  $T = 0$  state located at 1519 keV. Observed coincidences illustrated in Figs. 8(a) and 8(b) and in Fig. 10(a) all show a peak at 960 keV, which corresponds exactly to the energy difference between the 2479- and 1519-keV levels. The angular distribution coefficient and ratio suggest  $E2$  character for the 556-keV transition, which implies that the state at 1519 keV is  $4_1^+$ . This would lead to the fact that the 960-keV transition from the 2479-keV,  $5_4^+$  state to the 1519-keV,  $4_1^+$  state should be  $M1$  type. Unfortunately, it was not possible to extract the  $R$  value with small-enough uncertainty to fix the multipolarity of the 960-keV transition. Therefore, the level at 1519 keV is only tentatively assigned as  $I = 4$ .

### 3. The ( $T = 1, 6^+$ ) state at 3674 keV

One of the most prominent peaks presented in Fig. 7(b), located at 836–841 keV, is most probably a triplet. As previously mentioned, the 836-keV line represents the transition from the  $1_1^+$  state in Band 3 and the formerly known 841-keV  $\gamma$ -ray transition feeds the isomeric  $9_1^+$  state [9] in Band 4. Looking at the coincidences illustrated in Figs. 8(a), 8(c), and 10(a), a line at 840 keV can be observed in each of the figures, which cannot be associated with either of the two previously mentioned  $\gamma$ -ray transitions. After fixing most of the levels within the  $T = 1$  and different  $T = 0$  bands, the 840-keV line fits within error limits between the  $T = 0$ ,  $7_2^+$  and tentative  $T = 1$ ,  $6_1^+$  levels located at 2833 and 3674 keV, respectively, and satisfies the observed coincidences. The angular distribution ratio [ $R = 0.60(21)$ ], which is consistent with a stretched  $M1$  transition, is derived for the 840-keV line because it can be effectively separated from the other members of the triplet by clean  $\gamma\gamma$  coincidence relations.

### 4. Short-lived structures above the isomeric states

The recoil-isomer tagging method [38,39] was employed both alone and in conjunction with the  $\beta$ -tagging method. Prompt structures above the isomeric  $9_1^+$  state, previously reported in Ref. [9], were also observed in the present study and the ordering confirmed on the basis of  $\gamma\gamma$  analysis. The 841-keV transition is clearly the most intense, as can be noted from Fig. 11(a). Therefore, it has to be feeding the isomeric  $9_1^+$  state at 3021 keV. Both the angular distribution coefficient [ $A_2 = 0.30(5)$ ] and ratio [ $R = 1.17(3)$ ] deduced for the 841-keV transition are typical for an  $E2$  transition. This leads to a spin assignment of  $11_1^+$  for the level at 3862 keV. A second intense transition in Fig. 11(a) is the 1462-keV line with angular distribution values indicating an  $E2$  character. A strong mutual coincidence observed between the 841- and 1462-keV lines suggests that the latter transition feeds the  $11_1^+$  state and depopulates a  $13_1^+$  level at 5325 keV; hence, they belong to the same  $T = 0$  band. The 1206-keV transition is observed in coincidence with both of the previously mentioned lines and the extracted angular distribution ratio implies  $M1$  character. The 1206-keV transition is therefore assigned tentatively to depopulate a  $14_1^+$  state at 6530 keV, in good agreement with Ref. [9]. The 722-keV transition [ $R = 1.49(28)$ ] is observed

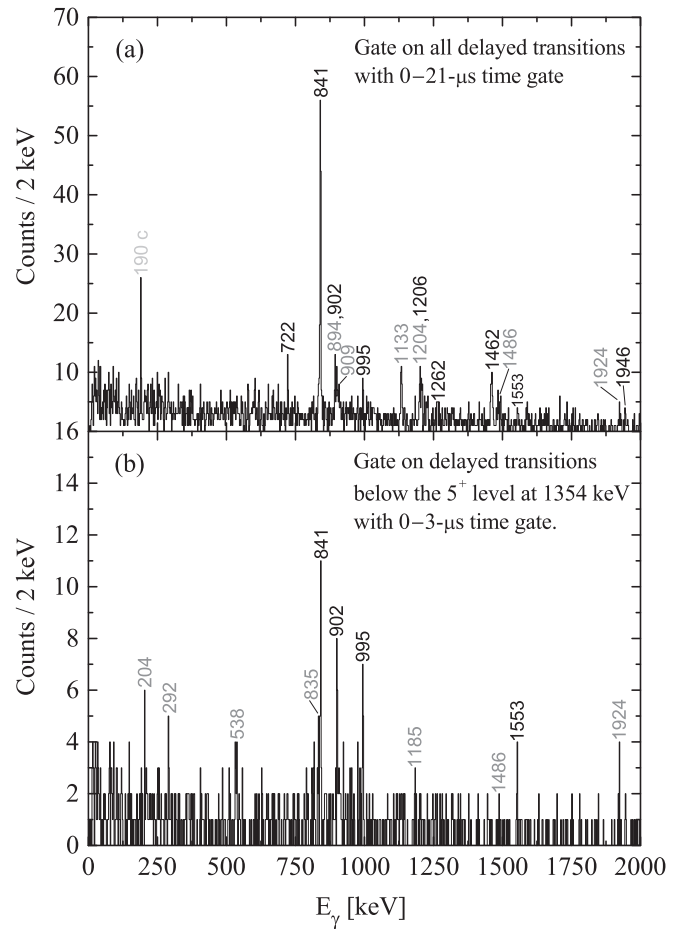


FIG. 11. Recoil-isomer and  $\beta$ -tagged JUROGAM II singles spectra. In panel (a) all delayed  $\gamma$ -ray transitions associated with  $^{66}\text{As}$  are used as a tag with the  $\beta$ -energy gate of 1.5–10 MeV. In panel (b) only the delayed  $\gamma$ -ray transitions originating from states below the lower-lying isomeric  $5_1^+$  state in  $^{66}\text{As}$  are used as a tag along with a  $\beta$  gate of 1.5–10 MeV. Peaks labeled in dark gray are unidentified transitions while the peak labeled in gray and marked with a “c” is a contaminant from  $^{65}\text{Ga}$ .

in coincidence with the 841-keV line simultaneously with the 1946- and 1262-keV transitions, but not with the relatively strong 1206- and 1462-keV transitions. The 722-keV transition is tentatively assigned to deexcite the  $14_1^+$  state at 6530 keV and to feed a  $12_1^+$  state at 5808 keV, which in turn is deexcited by the 1946-keV transition.

Peaks labeled in gray in Figs. 11(a) and 11(b) are  $\gamma$ -ray transitions, which could not be associated with any of the competing reaction products nor linked with the other observed  $^{66}\text{As}$   $\gamma$ -ray transitions. The 894-, 909-, and 1133-keV transitions were also reported in Ref. [9] but the authors were unable to place them in the level scheme.

Figure 11(b) shows a  $\beta$ - and isomer-tagged JUROGAM II singles spectrum with 0- to 3- $\mu\text{s}$   $\gamma$ -recoil time gate suitable for the lower-lying  $5_1^+$  isomeric state. Three intense peaks at 841, 902, and 995 keV are observed. The latter two were confirmed to be in mutual coincidence, but could not be connected to any other prompt  $\gamma$ -ray transitions found in  $^{66}\text{As}$ . The 902- and 995-keV transitions were investigated with very strict  $\beta$  and

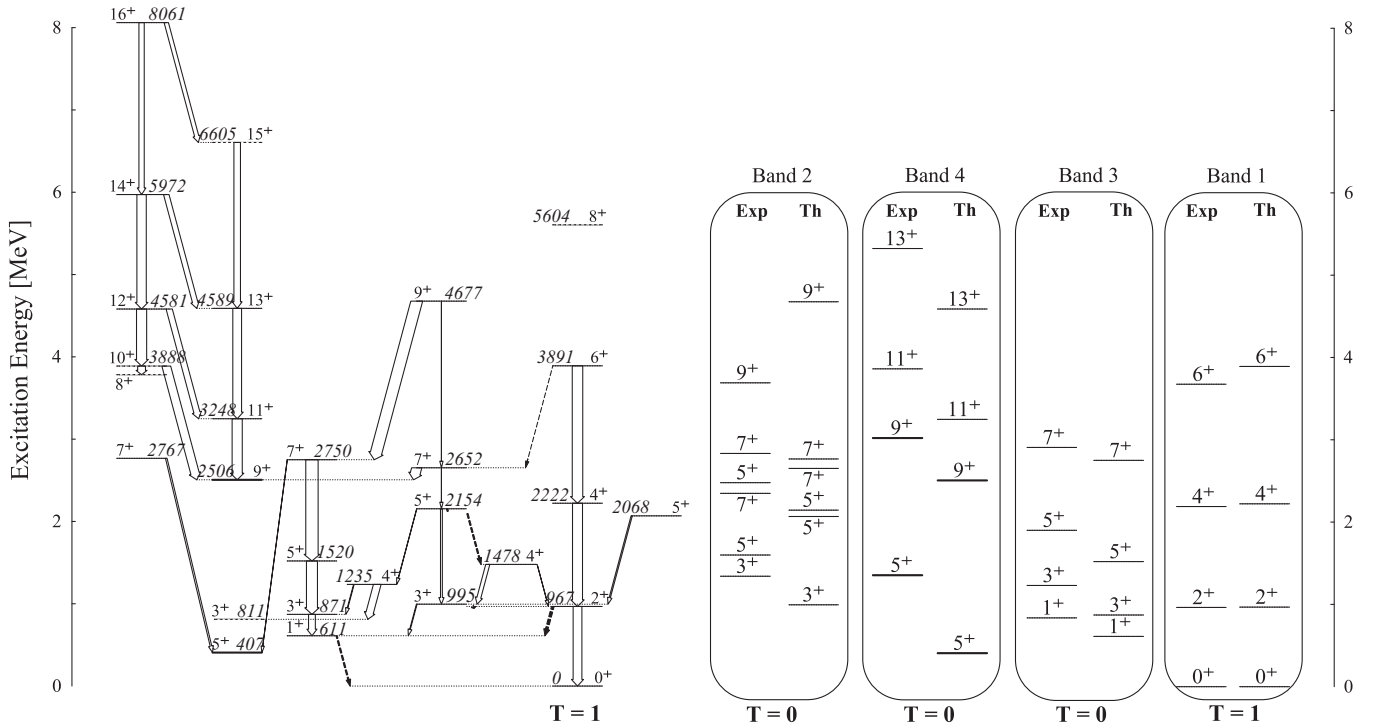


FIG. 12. (Left) The energy levels of  $^{66}\text{As}$  predicted by the present SM calculation. The width of the arrow corresponds to the relative value of the calculated  $E2$  (solid arrow) and  $M1$  (dashed arrow) transition strengths. The dashed levels are theoretically predicted but not observed in the experiment. (Right) Comparison of the experimental (Exp) and theoretical (Th) level energies for the  $T = 1$  (right) and different  $T = 0$  sequences.

time gates and can be unambiguously associated with  $^{66}\text{As}$ . As the 995-keV transition is found to be slightly more intense than the 902-keV transition, the 995-keV line is assigned to feed directly to the isomeric  $5_1^+$  state. The angular distribution ratios obtained both for the 902- and 995-keV lines, favor  $E2$  type of transitions; thus, the levels at 2349 and 3251 keV are tentatively assigned as  $7_1^+$  and  $9_2^+$ , respectively. There seems to be a small peak at 835 keV right next to the 841-keV peak as illustrated in Fig. 11(b). In addition, there are some events detected around 1486 keV, which are visible in both panels of Fig. 11. One could speculate that a 835-keV  $M1$  transition from a  $T = 1$ ,  $4_3^+$  state could feed directly in the isomeric  $5_1^+$  state. However, this scenario could not be confirmed unambiguously during the data analysis; hence, it will be left as an open question.

#### IV. DISCUSSION

The structure of  $^{66}\text{As}$  has been studied theoretically by Hasegawa *et al.* [36] and Honma *et al.* [12]. Both of these studies were based on SM calculations using the  $2p_{3/2}$ ,  $1f_{5/2}$ ,  $2p_{1/2}$ , and  $1g_{9/2}$  single-particle orbits as a model space. Differences between these calculations arise mainly from the interaction used and the single-particle energies. Identical calculations as applied in Ref. [12] using the modern effective JUN45 interaction have been employed in the present work to compare with the experimental data. These calculations were extended beyond the isomeric structures to include properties of all states and  $E2/M1$  transition strengths. The resulting theoretical level energies are illustrated in Fig. 12.

#### A. Isomeric states and $E2$ transition strengths

Studies presented in Refs. [36] and [12] both suggest that the structure of the experimentally observed isomeric  $9_1^+$  and  $5_1^+$  states can be interpreted as fully aligned proton-neutron pairs in the  $g_{9/2}$  and  $f_{5/2}$  orbitals, respectively. This conclusion seems to be valid according to the experimentally confirmed spins and parities of these states. It is interesting to compare the different theoretical  $E2$  transition strengths for the  $9_1^+ \rightarrow 7_3^+$  and  $5_1^+ \rightarrow 3_1^+$  transitions with the ones derived from the experimental lifetimes and conversion coefficients. The corresponding  $B(E2)$  values are listed in Table III, where experimental  $B(E2)$  values, as reported in Ref. [8], are also included for comparison. It should be noted that those values are derived from experimental half-lives (superseded later in Ref. [9]) and conversion coefficients.

TABLE III. Comparison of experimental and SM-predicted  $\gamma$ -ray transition strengths for  $^{66}\text{As}$ .

| $I_i^\pi \rightarrow I_f^\pi$ | $B(E2; I_i^\pi \rightarrow I_f^\pi) (e^2 \text{ fm}^4)$ |       |        |          |
|-------------------------------|---|-------|--------|----------|
|                               | Exp.  | JUN45 | EPQQM  | Ref. [8] |
| $9_1^+ \rightarrow 7_3^+$     | 2.6(3)  | 0.22  | 0.36   | 0.7(1)   |
| $5_1^+ \rightarrow 3_1^+$     | 13(2)   | 16.02 | 117.24 | 5.4(14)  |
|                               | $B(E2; I_i^\pi \rightarrow I_f^\pi) (\text{W.u.})$      |       |        |          |
| $9_1^+ \rightarrow 7_3^+$     | 0.16(2)   | 0.014 | 0.023  | 0.044(6) |
| $5_1^+ \rightarrow 3_1^+$     | 0.8(1)  | 1.01  | 7.40   | 0.34(9)  |

TABLE IV. Nucleon occupation numbers of orbitals in the four model-space orbits for low-lying  $T = 1$  and  $T = 0$  states in  $^{66}\text{As}$ .

| $I_i^{\pi}, T$ | $n_{ij}^{\pi} = n_{ij}^{\nu}$ |           |           |           |
|----------------|-------------------------------|-----------|-----------|-----------|
|                | $p_{3/2}$                     | $f_{5/2}$ | $p_{1/2}$ | $g_{9/2}$ |
| $9_1^+, 0$     | 1.606                         | 1.857     | 0.461     | 1.076     |
| $9_2^+, 0$     | 2.081                         | 2.189     | 0.537     | 0.194     |
| $7_1^+, 0$     | 1.589                         | 1.869     | 0.474     | 1.068     |
| $7_2^+, 0$     | 2.198                         | 2.037     | 0.528     | 0.237     |
| $6_1^+, 1$     | 2.300                         | 1.825     | 0.569     | 0.306     |
| $5_1^+, 0$     | 2.739                         | 1.230     | 0.853     | 0.178     |
| $5_2^+, 0$     | 2.320                         | 1.855     | 0.575     | 0.250     |
| $4_3^+, 1$     | 2.416                         | 1.643     | 0.623     | 0.318     |
| $3_2^+, 0$     | 2.460                         | 1.682     | 0.612     | 0.246     |

The extended P + QQ interaction with monopole corrections (hereafter called EPQQM) used in Ref. [36] produces  $B(E2)$  values, which differ approximately by factors of 0.1 and 10 with the respective experimental values. The experimental level energies of the isomeric  $9_1^+$  and  $5_1^+$  states are, however, roughly reproduced by the calculation. The present calculation using the JUN45 interaction produces a  $B(E2; 5_{1,\text{th}}^+ \rightarrow 3_{2,\text{th}}^+)$  value, which agrees well with the experimental one, suggesting that the model correctly describes the wave functions of the states involved in the transition. Nevertheless, the predicted level energy for the isomeric  $5_{1,\text{th}}^+$  state is 0.95 MeV below the experimental counterpart. The theoretical  $B(E2; 9_{1,\text{th}}^+ \rightarrow 7_{2,\text{th}}^+)$  is again too low by factor of 10 and the  $9_{1,\text{th}}^+$  level energy is 0.52 MeV below the experimental isomeric  $9_1^+$  state.

Nucleon occupancies of orbitals from present SM calculation are presented in Table IV. This theoretical study and the one presented in Ref. [36] both predict  $\sim 20\%$  occupation of valence nucleons in the  $g_{9/2}$  orbit in the case of the isomeric  $9_{1,\text{th}}^+$  state, while for the other calculated levels the  $g_{9/2}$  occupation is, on average, only 3%–6%. This is especially true for the theoretical  $7_{2,\text{th}}^+$  state, which the isomeric  $9_{1,\text{th}}^+$  state is expected to decay into. This result implies that the isomerism of the  $9_{1,\text{th}}^+$  state is indeed attributable to its structural difference compared to the  $7_{2,\text{th}}^+$  state. However, the present SM calculation predicts another  $7_{1,\text{th}}^+$  state with almost identical orbital occupancies as obtained for the isomeric  $9_{1,\text{th}}^+$  state. This structural similarity is naturally reflected in the pronounced  $E2$  transition strength, which is of the order of  $460 e^2 \text{fm}^4$ . Taking this fact into account and remembering the theoretical underestimation of the  $B(E2; 9_{1,\text{th}}^+ \rightarrow 7_{2,\text{th}}^+)$  value, one can speculate whether the mixing of the different  $7^+$  states is correctly reproduced by the theory. Alternatively, the effect of the  $g_{9/2}$  orbit on the structure of excited states in  $^{66}\text{As}$  could possibly be refined. The isomerism of the  $5_1^+$  is not likely to originate from major structural differences, at least in the light of calculated orbital occupation numbers, but can simply be explained by the low decay energy.

### B. Oblate $3^+$ shape isomer

The existence of a  $3_{1,\text{th}}^+$  shape isomer was predicted in Ref. [36]. The prediction of the isomerism arises from the

calculated quadrupole moments from which one can infer an oblate shape for the  $3_{1,\text{th}}^+$  state and prolate shapes for the other low-lying states. However, the predicted isomeric state was not found in the present study. The experimental setup used in this work has certain limitations to observe fast decays. This is attributable to the  $\sim 500$ -ns flight time of fusion residues through the RITU separator. This limit is cross-section dependent, but if the isomer exists, the lifetime of the state should be of the order of  $> 100$  ns to be observed at the focal plane of RITU. Also, the 10-ns time resolution of TDR does not permit the investigation of small time differences of the  $\gamma$  rays measured at the JUROGAM II target position.

Recent experimental work on  $^{66}\text{As}$  reported in Ref. [10], led to the discovery of a  $3_2^+$  state with a 1.1(3)-ns half-life, which was determined on the basis of the centroid-shift method [40]. This state is proposed to be the predicted oblate shape isomer and is deexcited by a strong 379-keV  $M1$  and a weaker 506-keV and a nonobserved 112-keV  $\gamma$ -ray transition. In the present study a  $3_2^+$  state, which is deexcited similarly by the strong 379-keV  $M1$  and weaker 506-keV ( $E2$ )  $\gamma$ -ray transitions, was identified. It is reasonable to assume that it is the same  $3_2^+$  state, which has been successfully discovered in both experiments. However, no 112-keV  $\gamma$  rays originating from  $^{66}\text{As}$  were observed in the present study. In Ref. [10] the nonobservation of the 112-keV transition is explained by the germanium array detection efficiency, which was reduced owing to the strong absorption in the CsI charged particle ancillary detectors used in that experiment. With the JUROGAM II array such limitations were not present and therefore the reported 112-keV transition with 6% intensity should have been observed.

If the  $3_2^+$  state has  $\sim 1$ -ns half-life, the  $\gamma$ -ray emission should take place 0–30 mm downstream from the JUROGAM II target position. This would cause a slight drop in the detection efficiency of the 379- and 506-keV  $\gamma$  rays, but more importantly, the change in the detection angle would lead to an incorrect Doppler correction or a shift of a few keV in the measured  $\gamma$ -ray energy in the  $75.5^\circ$  and  $104.5^\circ$  JUROGAM II rings. This should be observable in the  $\gamma$ -ray spectrum as a broadened or skewed peak shape. The peak shapes of the 355-, 379-, and 394-keV transitions were examined but no differences in their respective shapes were observed.

### C. $T = 1$ and $T = 0$ states in $^{66}\text{As}$

The present SM calculation produces the level energies of the  $T = 1$ ,  $2_1^+$  (967 keV),  $4_3^+$  (2222 keV), and  $6_1^+$  (3891 keV) states in relatively good agreement with the experimental  $2_1^+$  (963 keV),  $4_3^+$  (2189 keV), and  $(6_1^+)$  (3674 keV) states (see Fig. 12). Recent theoretical work by Kaneko *et al.* [11], which again is based on calculations identical to those used in the present work, predicts the CED between the  $T = 1$  states in odd-odd  $N = Z$  systems and their analog even-even partners. Recent experimental work on  $^{66}\text{As}$  [10] proposes a  $T = 1$ ,  $6_1^+$  state at an energy of 3637 keV, which results in the initially positive CED trend between  $^{66}\text{As}/^{66}\text{Ge}$  having a sudden negative gradient at spin  $6\hbar$ . In Ref. [10] this unusual behavior, along with the unique negative CED trend observed

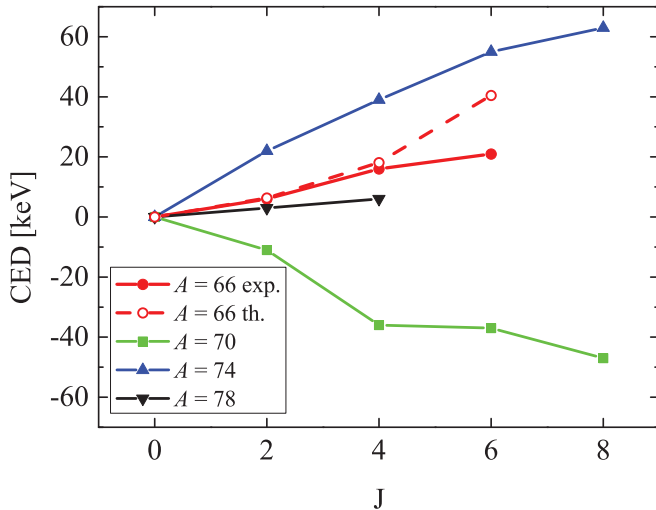


FIG. 13. (Color online) The experimental CED systematics for the mass  $A = 66, 70, 74,$  and  $78$  systems (solid lines). The calculated CED with JUN45 interaction for the mass  $A = 66$  pair is shown as dashed line to compare with the experimental data. Data are taken from Refs. [6,37,41–43].

within the  $A = 70$  pair ( $^{70}\text{Br}/^{70}\text{Se}$ ), was accounted for by the different mixing of competing shapes between the isobaric analog states. However, in Ref. [11] the SM calculations correctly reproduce the negative CED trend for the  $A = 70$  pair with a nearly static oblate deformation in  $^{70}\text{Se}$ . The main reason for the anomalous trend in the latter work is found to be the enhanced neutron and reduced proton excitations to the  $g_{9/2}$  orbit owing to the electromagnetic spin-orbit interaction. In the present work, the candidate for the  $T = 1, 6_1^+$  state is found to lie at 3674 keV, 37 keV higher than proposed in Ref. [10]. This leads to a moderately positive CED behavior within the  $A = 66$  pair, as illustrated in Fig. 13. A similar trend is also predicted by the present theoretical calculation, if one particularly considers the first  $6_{\text{th}}^+$  states (see Fig. 13). Figure 13 shows also heavier systems for comparison. In the case of the mass  $A = 74$  and  $78$  pairs, large positive and almost flat CED trends are observed, respectively. Generally, the positive CED trends are explained by the Coriolis antipairing, i.e., breaking of valence nucleon pairs when angular momentum is generated [6]. This causes the even-even  $N = Z - 2$  partner to have a greater reduction in Coulomb energy because it has more  $pp$  pairs than the odd-odd  $N = Z$  partner of the multiplet. In the case of the  $A = 78$  pair, an almost flat CED is proposed to be attributable to the deformed shell gap at  $Z, N = 38$ , which inhibits shape changes and suppresses pairing effects [44]. The observed CED trend for the  $A = 66$  pair is only slightly steeper than the one observed for the  $A = 78$  pair. Clearly, the  $Z, N = 38$  shell gap should not have much of an influence in the case of  $^{66}\text{As}$ . In addition, taking into account the recent theoretical result for the mass  $A = 70$  pair, coexisting shapes may not necessarily be the origin of the observed flatness in the CED behavior in the case of the mass  $A = 66$  pair. In Ref. [11] the single-particle energy shift component, which is greatly affected by the electromagnetic spin-orbit interaction, is found to flatten the CED trend for the  $A = 66$  system, as

it is purely negative as in the case of the  $A = 70$  pair. This hints toward the importance of the  $g_{9/2}$  orbit and its interplay with the  $fp$ -shell orbits in the structure of the  $^{66}\text{As}$ . Further discussion of CED and their implications around the  $N = Z$  line will be carried out in a future publication [45], where new results on the full  $A = 66$  isospin triplet will be presented.

In Fig. 2 the tentative 840-keV  $\gamma$ -ray transition connecting the supposed  $6_1^+$  state and the  $7_2^+$  is very interesting. The quasideuteron description [46] can be used to estimate and predict the isovector  $M1$  transition strengths in odd-odd  $N = Z$  nuclei. According to this approximation, the  $M1$  transition strength is greatly dependent on the characteristics of the single-particle orbits contributing to the level configuration. In the case of  $j = l + 1/2$  orbitals, the spin of the nucleon and orbital angular momentum are aligned and strong isovector  $M1$  transitions are favored. If the single-particle orbital is of type  $j = l - 1/2$ , the spin and orbital parts are out of phase, resulting in small  $M1$  matrix elements. Obviously, as the low-lying excitations in  $^{66}\text{As}$  are presumably mainly based on the  $f_{5/2}$  ( $j = l - 1/2$ ) and  $p_{3/2}$  ( $j = l + 1/2$ ) configurations, a strong  $M1$  transition between the lowest  $T = 0$  and  $T = 1$  states, i.e., between  $2_1^+$  and  $1_1^+$ , is experimentally missing. The situation, however, might be different at higher values of angular momentum. As already noticed in the case of the  $9_1^+$  isomeric state, the importance of the  $g_{9/2}$  ( $j = l + 1/2$ ) orbit becomes evident. If one considers the situation where the amplitude of the  $g_{9/2}$  component increases along with the spin within the  $T = 1$  band, the  $M1$  transitions might become the dominant decay mechanism over the  $E2$  transitions. This might be the case for the  $6_1^+$  state where the 840-keV  $\gamma$ -ray branch to the  $T = 0, 7_2^+$  state is greater (82%) than the 1486-keV  $\gamma$ -ray branch feeding the  $T = 1, 4_3^+$  state (18%). The  $B(M1)$  value for the  $6_1^+ \rightarrow 7_2^+$  transition can be estimated in a manner similar to that used in Ref. [47] by using the experimental branching ratio and recently measured  $B(E2; 2_1^+ \rightarrow 0_1^+)$  value in  $^{66}\text{Ge}$  [48]. Assuming the  $B(E2)$  value does not significantly change between higher lying  $T = 1$  states in  $^{66}\text{Ge}$ , the  $B(M1; 6_1^+ \rightarrow 7_2^+)$  value is estimated to be  $\sim 1\mu_N^2$ , which is surprisingly large. The present SM calculation does not support this scenario in terms of  $M1$  transition strengths and  $g_{9/2}$  occupancy (see Table IV). If the monopole matrix elements are correctly described by the theory, this should lead to a rather high  $M1$  transition strength in the case of the  $3_2^+$  state decay to explain the experimentally observed favoring of the  $M1$  branch over the  $E2$  branch, but such enhancement was not predicted.

The theoretically predicted level energies of the low-lying  $T = 0$  states are in relatively good agreement with the experimental ones. The agreement is particularly good in the case of Band 3 ( $T = 0$ ), which is connected to the isomeric states. The theory predicts three  $7^+$  states with similar energies, which agrees extremely well with the experimental data. The theoretical description fails in the case of Band 4 and 5 in terms of excitation energy and level spacings. Despite the daunting task of theoretically describing odd-odd  $N = Z$  systems, the current model is found to do very well in the case of the low-lying excitations of  $^{66}\text{As}$ . This fact is reflected in the experimental and theoretical  $B(E2; 5_1^+ \rightarrow 3_1^+)$  values, which are in remarkable agreement.

## V. SUMMARY

The odd-odd  $N = Z$  nucleus  $^{66}\text{As}$  has been experimentally studied in detail. Prompt and delayed structures have been observed utilizing RBT and recoil-isomer tagging methods. The half-lives of two isomeric states and the internal conversion coefficients of the  $\gamma$  rays depopulating these levels were measured with improved accuracy, yielding the experimental  $B(E2)$  values. Some of the newly observed prompt  $\gamma$ -ray transitions were also identified in Ref. [10]. The arrangement of the  $\gamma$ -ray transitions differs slightly between these two studies, especially within  $T = 0$  structures. The level energies of the  $T = 1$ ,  $2_1^+$ , and  $4_3^+$  states are established in agreement with the ones reported in Ref. [10]. However, the candidates for the  $T = 1$ ,  $6_1^+$  state differ in terms of level energy. Depending on which one of the experimental  $6_1^+$  energies is used, a somewhat different behavior in the CED trend is obtained. The SM calculations using the effective JUN45 interaction predicts that the CED should have a positive trend, which is consistent with the current data. Low-lying  $T = 0$  states are described well by theory in terms of excitation energy when

compared to the experimental counterparts. The same holds for the  $T = 1$  band members. A disagreement between experiment and theory was found for the  $B(E2)$  and  $B(M1)$  strengths for the  $9_1^+ \rightarrow 7_3^+$  and  $6_1^+ \rightarrow 7_2^+$  transitions, respectively. This discrepancy is most likely attributable to theory not correctly reproducing the behavior of the  $g_{9/2}$  orbit at higher spins.

## ACKNOWLEDGMENTS

This work was supported by the Academy of Finland under the Finnish Centre of Excellence Programme and by the UK Science and Technology Facilities Council (STFC). The authors would like to thank the GAMMAPOOL European Spectroscopy Resource for the loan of germanium detectors for JUROGAM II. This work has also benefited from the use of TNT2-D cards, developed and financed by CNRS/IN2P3 for the GABRIELA project. P.R. acknowledges Magnus Ehrnrooth foundation for the support for this work and the GRASPANP for the travel support.

- 
- [1] B. Cederwall *et al.*, *Nature (London)* **469**, 68 (2011).  
 [2] B. S. Nara Singh *et al.*, *Phys. Rev. Lett.* **107**, 172502 (2011).  
 [3] I. Mukha *et al.*, *Nature (London)* **439**, 298 (2006).  
 [4] M. A. Bentley and S. M. Lenzi, *Prog. Part. Nucl. Phys.* **59**, 497 (2007).  
 [5] P. E. Garrett, W. E. Ormand, D. Appelbe, R. W. Bauer, J. A. Becker, L. A. Bernstein, J. A. Cameron, M. P. Carpenter, R. V. F. Janssens, C. J. Lister *et al.*, *Phys. Rev. Lett.* **87**, 132502 (2001).  
 [6] B. S. Nara Singh, A. N. Steer, D. G. Jenkins, R. Wadsworth, M. A. Bentley, P. J. Davies, R. Glover, N. S. Pattabiraman, C. J. Lister, T. Grahn *et al.*, *Phys. Rev. C* **75**, 061301(R) (2007).  
 [7] S. M. Lenzi, N. Märginean, D. R. Napoli, C. A. Ur, A. P. Zuker, G. de Angelis, A. Algora, M. Axiotis, D. Bazzacco, N. Belcari *et al.*, *Phys. Rev. Lett.* **87**, 122501 (2001).  
 [8] R. Grzywacz, S. Andriamonje, B. Blank, F. Boué, S. Czajkowski, F. Davi, R. D. Moral, C. Donzaud, J. Dufour, A. Fleury *et al.*, *Phys. Lett. B* **429**, 247 (1998).  
 [9] R. Grzywacz, C. Yu, Z. Janas, S. Paul, J. Batchelder, C. Bingham, T. Ginter, C. Gross, J. McConnell, M. Lipoglavšek *et al.*, *Nucl. Phys. A* **682**, 41c (2001).  
 [10] G. de Angelis, K. T. Wiedemann, T. Martinez, R. Orlandi, A. Petrovici, E. Sahin, J. J. Valiente-Dobón, D. Tonev, S. Lunardi, B. S. Nara Singh *et al.*, *Phys. Rev. C* **85**, 034320 (2012).  
 [11] K. Kaneko, T. Mizusaki, Y. Sun, S. Tazaki, and G. de Angelis, *Phys. Rev. Lett.* **109**, 092504 (2012).  
 [12] M. Honma, T. Otsuka, T. Mizusaki, and M. Hjorth-Jensen, *Phys. Rev. C* **80**, 064323 (2009).  
 [13] A. Steer, D. Jenkins, R. Glover, B. N. Singh, N. Pattabiraman, R. Wadsworth, S. Eeckhaudt, T. Grahn, P. Greenlees, P. Jones *et al.*, *Nucl. Instrum. Methods Phys. Res., Sect. A* **565**, 630 (2006).  
 [14] J. Henderson, P. Ruotsalainen, D. Jenkins, C. Scholey, K. Auranen, P. Davies, T. Grahn, P. Greenlees, T. Henry, A. Herzáň *et al.*, *J. Inst.* **8**, P04025 (2013).  
 [15] G. Duchêne, F. Beck, P. Twin, G. de France, D. Curien, L. Han, C. Beausang, M. Bentley, P. Nolan, and J. Simpson, *Nucl. Instrum. Methods Phys. Res., Sect. A* **432**, 90 (1999).  
 [16] C. Beausang, S. Forbes, P. Fallon, P. Nolan, P. Twin, J. Mo, J. Lisle, M. Bentley, J. Simpson, F. Beck *et al.*, *Nucl. Instrum. Methods Phys. Res., Sect. A* **313**, 37 (1992).  
 [17] C. Rossi Alvarez, *Nucl. Phys. News* **3**, 10 (1993).  
 [18] M. Leino, J. Äystö, T. Enqvist, P. Heikkinen, A. Jokinen, M. Nurmi, A. Ostrowski, W. Trzaska, J. Uusitalo, K. Eskola *et al.*, *Nucl. Instrum. Methods Phys. Res., Sect. B* **99**, 653 (1995).  
 [19] J. Sarén, J. Uusitalo, M. Leino, and J. Sorri, *Nucl. Instrum. Methods Phys. Res., Sect. A* **654**, 508 (2011).  
 [20] R. Page, A. Andreyev, D. Appelbe, P. Butler, S. Freeman, P. Greenlees, R.-D. Herzberg, D. Jenkins, G. Jones, P. Jones *et al.*, *Nucl. Instrum. Methods Phys. Res., Sect. B* **204**, 634 (2003).  
 [21] I. Lazarus, D. Appelbe, P. Butler, P. Coleman-Smith, J. Cresswell, S. Freeman, R. Herzberg, I. Hibbert, D. Joss, S. Letts *et al.*, *IEEE Trans. Nucl. Sci.* **48**, 567 (2001).  
 [22] P. Rahkila, *Nucl. Instrum. Methods Phys. Res., Sect. A* **595**, 637 (2008).  
 [23] D. C. Radford, *Nucl. Instrum. Methods Phys. Res., Sect. A* **361**, 297 (1995).  
 [24] D. C. Radford, *Nucl. Instrum. Methods Phys. Res., Sect. A* **361**, 306 (1995).  
 [25] R. H. Burch Jr., C. A. Gagliardi, and R. E. Tribble, *Phys. Rev. C* **38**, 1365 (1988).  
 [26] D. E. Alburger, *Phys. Rev. C* **18**, 1875 (1978).  
 [27] M. J. López Jiménez, B. Blank, M. Chartier, S. Czajkowski, P. Dessagne, G. de France, J. Giovinazzo, D. Karamanis, M. Lewitowicz, V. Maslov, C. Miehle, P. H. Regan, M. Stanoiu, and M. Wiescher, *Phys. Rev. C* **66**, 025803 (2002).  
 [28] C. N. Davids, *IEEE Trans. Nucl. Sci.* **26**, 1191 (1979).  
 [29] W. E. Ormand, *Phys. Rev. C* **55**, 2407 (1997).  
 [30] K.-H. Schmidt, C.-C. Sahm, and H.-G. C. K. Pielenz, *Z. Phys. A* **316**, 19 (1984).  
 [31] K. H. Schmidt, *Eur. Phys. J. A* **8**, 141 (2000).

- [32] M. R. Bhat and J. K. Tuli, *Nucl. Data Sheets* **90**, 269 (2000).
- [33] E. Browne and J. K. Tuli, *Nucl. Data Sheets* **111**, 2425 (2010).
- [34] S. Agostinelli *et al.*, *Nucl. Instrum. Methods Phys. Res., Sect. A* **506**, 250 (2003).
- [35] T. Kibédi, T. Burrows, M. Trzhaskovskaya, P. Davidson, and C. Nestor, Jr., *Nucl. Instrum. Methods Phys. Res., Sect. A* **589**, 202 (2008).
- [36] M. Hasegawa, Y. Sunb, K. Kaneko, and T. Mizusaki, *Phys. Lett. B* **617**, 150 (2005).
- [37] E. A. Stefanova, I. Stefanescu, G. de Angelis, D. Curien, J. Eberth, E. Farnea, A. Gadea, G. Gersch, A. Jungclaus, K. P. Lieb *et al.*, *Phys. Rev. C* **67**, 054319 (2003).
- [38] D. M. Cullen, N. Amzal, A. J. Boston, P. A. Butler, A. Keenan, E. S. Paul, H. C. Scraggs, A. M. Bruce, C. M. Parry, J. F. C. Cocks *et al.*, *Phys. Rev. C* **58**, 846 (1998).
- [39] C. Scholey, D. M. Cullen, E. S. Paul, A. J. Boston, P. A. Butler, T. Enqvist, C. Fox, H. C. Scraggs, S. L. Shepherd, O. Stezowski *et al.*, *Phys. Rev. C* **63**, 034321 (2001).
- [40] R. Orlandi, G. de Angelis, P. G. Bizzeti, S. Lunardi, A. Gadea, A. M. Bizzeti-Sona, A. Bracco, F. Brandolini, M. P. Carpenter, C. J. Chiara *et al.*, *Phys. Rev. Lett.* **103**, 052501 (2009).
- [41] G. de Angelis, T. Martinez, A. Gadea, N. Marginean, E. Farnea, E. Maglione, S. Lenzi, W. Gelletly, C. Ur, D. Napoli *et al.*, *Eur. Phys. J. A* **12**, 51 (2001).
- [42] G. Rainovski, H. Schnare, R. Schwengner, C. Plettner, L. Käubler, F. Dönau, I. Ragnarsson, J. Eberth, T. Steinhardt, O. Thelen *et al.*, *J. Phys. G: Nucl. Part. Phys.* **28**, 2617 (2002).
- [43] F. Johnston-Theasby, A. V. Afanasjev, C. Andreoiu, R. A. E. Austin, M. P. Carpenter, D. Dashdorj, S. J. Freeman, P. E. Garrett, J. Greene, A. Görgen *et al.*, *Phys. Rev. C* **78**, 034312 (2008).
- [44] D. Rudolph, C. Baktash, C. J. Gross, W. Satula, R. Wyss, I. Birriel, M. Devlin, H.-Q. Jin, D. R. LaFosse, F. Lerma *et al.*, *Phys. Rev. C* **56**, 98 (1997).
- [45] P. Ruotsalainen *et al.*, *Phys. Rev. Lett.* (submitted).
- [46] A. F. Lisetskiy, R. V. Jolos, N. Pietralla, and P. von Brentano, *Phys. Rev. C* **60**, 064310 (1999).
- [47] A. Schmidt, I. Schneider, C. Frießner, A. F. Lisetskiy, N. Pietralla, T. Sebe, T. Otsuka, and P. von Brentano, *Phys. Rev. C* **62**, 044319 (2000).
- [48] R. Lüttke, E. A. McCutchan, V. Werner, K. Aleksandrova, S. Atwater, H. Ai, R. J. Casperson, R. F. Casten, A. Heinz, A. F. Mertz *et al.*, *Phys. Rev. C* **85**, 017301 (2012).